

**NMR IMAGING TECHNIQUES AND APPLICATIONS  
IN THE FLOW BEHAVIOR OF FLUIDS IN POROUS MEDIA**

A Thesis  
By  
**HASSAN I. HALIMI**

Submitted to the Office of Graduate Studies of  
Texas A&M University  
in partial fulfillment of the requirements for the degree of  
**MASTER OF SCIENCE**

December 1990

Major Subject: Petroleum Engineering

**NMR IMAGING TECHNIQUES AND APPLICATIONS  
IN THE FLOW BEHAVIOR OF FLUIDS IN POROUS MEDIA**

A Thesis  
By  
HASSAN I. HALIMI

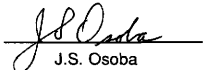
Approved as to style and content by:



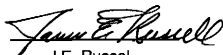
S.W. Poston  
(Chair of Committee)



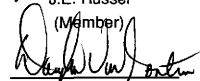
C.M. Edwards  
(Member)



J.S. Osoba  
(Member)



J.E. Russell  
(Member)



W.D. VonGonten  
(Head of Department)

December 1990

## ABSTRACT

NMR Imaging Techniques and Applications  
in the Flow Behavior of Fluids in Porous Media (December 1990)

Hassan I. Halimi, B.S., Texas A&M University  
Chair of Advisory Committee: Dr. S.W. Poston

NMR imaging techniques are based on the fact that nuclei will change their energy level when exposed to an external magnetic field. This research was conducted to study the flow behavior of fluids in porous media using this technique. A GECSI-II spectroscope was used to run the NMR experiments. A new inexpensive method of downloading and processing the raw NMR data files was developed. The new technique enabled a PC or a Macintosh to be used in place of much more expensive work-stations such as the Sun system.

A variety of public domain image processing software along with the in-house developed functions were used to process and enhance the saturation images produced by the NMR experiments. The NMR images resulting from the experiments represented the oil saturation in the core. An equation was developed to calculate both the oil and water saturations from the NMR image.

A relationship between relative permeability and gray-level distribution was also developed using the image saturation equation. An imbibition flooding experiment was carried out to visually study the flow behavior of oil while being displaced by water. The research provided a better understanding of the NMR theory and its applications in the flow behavior of fluids in porous media.

## **DEDICATION**

To my parents  
Ibrahim & Sohaila Halimi,  
whose love, support, and persistence  
kept me going.

## ACKNOWLEDGEMENTS

I wish to thank Dr. Steven W. Poston, Chair of my Advisory Committee, for his patience, understanding, and friendship throughout this study. I also wish to thank my committee members Dr. Edwards, Dr. Osoba, and Dr. Russell for their help and advice.

I wish to thank Mr. Hammad El-Harazin whose scholarship donation allowed me to attend Texas A&M University for the completion of my Bachelor's degree in Petroleum Engineering. I also wish to express my gratitude to Mr. Habib Jaradah and Mr. Zeyad Chrieh for their support. Thanks also go to my family and friends who provided my with emotional and spiritual support during my stay at Texas A&M.

I also would like to thank Mr. Jorge Perez for his help running the experiments. This study was funded by the Department of Energy and the State of Texas.

## TABLE OF CONTENTS

	Page
ABSTRACT.....	iii
DEDICATION .....	iv
ACKNOWLEDGEMENTS .....	v
TABLE OF CONTENTS .....	vi
LIST OF TABLES .....	x
LIST OF FIGURES .....	xi
<b>CHAPTER</b>	
<b>I INTRODUCTION .....</b>	<b>1</b>
1.1 Visualization Mechanism .....	1
1.2 NMR Research .....	2
1.3 Investigation Procedure .....	3
<b>II NUCLEAR MAGNETIC RESONANCE THEORY</b>	
<b>AND EXPERIMENT .....</b>	<b>5</b>
2.1 NMR Theory .....	5
2.1.1 Introduction .....	5
2.1.2 The Behavior of Nuclei in a Magnetic Field .....	6
2.1.3 Magnetization Behavior .....	12
2.1.4 Chemical Shift .....	17
2.1.5 Detection of Elements by the NMR .....	20
2.2 Relaxation and Fourier Transform .....	21
2.2.1 Spin-Lattice Relaxation .....	21
2.2.2 Spin-Lattice Relaxation Measurements .....	23
2.2.3 Spin-Spin Relaxation .....	24
2.2.4 Fourier Transform .....	26
2.3 NMR Components .....	30
2.3.1 NMR Types .....	30
2.3.2 Transmitter .....	31

## TABLE OF CONTENTS CONTINUED

CHAPTER	Page
2.3.3 Receiver .....	31
2.3.4 Magnets .....	33
2.3.5 Data Aquisition System .....	33
2.4 NMR Experiment .....	36
2.4.1 Applications of NMR Theory .....	36
2.4.2 Spectroscopy Experiments .....	41
2.4.3 Experimental Runs .....	44
2.4.4 Signal Processing .....	44
2.4.5 Preliminary Experimentation .....	44
2.4.6 Laboratory Experiment .....	46
III NUCLEAR MAGNETIC RESONANCE DATA PROCESSING .....	47
3.1 Introduction .....	47
3.1.1 Pattern Analysis .....	47
3.1.2 NMR Data .....	49
3.2 NMR Data Transformation .....	51
3.2.1 New Method .....	51
3.2.2 Experimental Data .....	52
3.2.3 Histogram Equalization .....	52
3.2.4 Example .....	58
3.2.5 Program .....	60
3.3 Image Processing Functions .....	66
3.3.1 Processing Methods .....	66
3.3.2 Spatial-Domain Methods .....	66
3.3.3 Frequency-Domain Methods .....	71
3.3.4 Local Enhancement .....	75
3.3.5 Image Smoothing .....	76
3.3.5.1 Neighborhood Averaging .....	76
3.3.5.2 Median Filtering .....	78

## TABLE OF CONTENTS CONTINUED

CHAPTER	Page
3.3.5.3 Low-Pass Filtering .....	78
3.3.6 Statistical Functions .....	81
3.3.6.1 Density Profile .....	81
3.3.6.2 Average Density Profile .....	81
3.3.6.3 Histogram Profile .....	81
3.3.6.4 Contour Maps .....	85
3.3.6.5 Saturation Front .....	85
3.3.6.6 Mean .....	85
3.3.6.7 3D Plot .....	85
3.4 Summary .....	92
3.4.1 Experimental Results .....	92
3.4.2 Image Saturation .....	92
IV APPLICATIONS OF NMR IN FLOW BEHAVIOR .....	98
4.1 Introduction .....	98
4.1.1 Reservoir Properties .....	98
4.1.2 Oil Saturation .....	99
4.1.3 Water Saturation .....	100
4.1.4 Permeability .....	101
4.1.5 Imbibition Flooding .....	102
4.1.6 Equipment Layout .....	103
4.2 Fluid Saturation .....	108
4.2.1 Methods of Measurements .....	108
4.2.2 Advantages of NMR Techniques .....	110
4.2.3 NMR Techniques .....	111
4.2.4 NMR Images .....	112
4.2.5 Image Saturation .....	112
4.2.6 Example .....	116



## TABLE OF CONTENTS CONTINUED

CHAPTER	Page
4.3 Relative Permeability .....	124
4.3.1 Multiphase Relative Permeability .....	124
4.3.2 Relative Permeability Measurements .....	124
4.3.3 Advantages of NMR on Permeability Measurements .....	126
4.3.4 Fluid Flow Theory .....	127
4.3.5 Measurements Procedure .....	129
4.3.6 Permeability From Well Logging .....	130
4.4 Imbibition Flooding .....	138
4.4.1 Imbibition Using NMR Techniques .....	138
4.4.2 Experimental Procedure .....	138
4.4.3 Image Analysis .....	139
4.4.4 Imbibition Study .....	147
 V SUMMARY AND CONCLUSIONS .....	 155
5.1 Summary .....	155
5.2 Conclusions.....	156
5.3 Recommendations .....	157
 NOMENCLATURE .....	 158
REFERENCES .....	159
APPENDIX A .....	163
APPENDIX B .....	166
APPENDIX C .....	170
VITA .....	171

**LIST OF TABLES**

	Page
Table 3.2.1 - Gray-level Distribution .....	59
Table 3.2.2 - Results of Transformation Function.....	59
Table 4.3.1 - Relative Permeability as a Function of Gray-level ( $S_{wi} = 0.15$ ) .....	132
Table 4.3.2 - Relative Permeability as a Function of Gray-level ( $S_{wi} = 0.20$ ) .....	133
Table 4.3.3 - Relative Permeability as a Function of Gray-level ( $S_{wi} = 0.25$ ) .....	134
Table 4.4.1 - Third Degree Saturation Function .....	150

## LIST OF FIGURES

	Page
Fig. 1.3.1	Diagram of the Procedure of Flow Behavior Study Using NMR Techniques .....4
Fig. 2.1.1	Two Energy Levels .....10
Fig. 2.1.2	Rotation of the Magnetic Moment About the Magnetic Field .....13
Fig. 2.1.3	Time and Frequency Domain Signals .....18
Fig. 2.1.4	Phase Shifting Using FT .....19
Fig. 2.2.1	Magnetization as a Function of Time .....25
Fig. 2.2.2	Sine Wave Transformation Using FT .....27
Fig. 2.2.3	NMR Spectrum .....29
Fig. 2.3.1	Major NMR Components .....32
Fig. 2.3.2	Transmitter .....32
Fig. 2.3.3	Receiver .....32
Fig. 2.3.4	The Operation of Phase Sensitive Detectors .....34
Fig. 2.3.5	NMR Spectroscopy (from Reference 16) .....35
Fig. 2.4.1	Rotation of the Magnetic Moment About the Magnetic Field.....37
Fig. 2.4.2	Magnetization Behavior .....40
Fig. 2.4.3	Free Induction Decay (FID) .....42
Fig. 2.4.4	NMR Signal Before Correction .....45
Fig. 2.4.5	NMR Signal After Correction .....45
Fig. 3.1.1	Statistical & Structural Methods .....48
Fig. 3.2.1	Example of NMR Raw Data File .....53
Fig. 3.2.2	Example of NMR Data File After Downloading .....54
Fig. 3.2.3	Typical Histogram .....56
Fig. 3.2.4	Density Function .....57
Fig. 3.2.5a	Original Histogram .....61
Fig. 3.2.5b	Transformation Function .....61
Fig. 3.2.5c	Equalized Histogram .....62
Fig. 3.2.6	Typical Equalization Mechanism .....64

## LIST OF FIGURES CONTINUED

		Page
Fig. 3.2.7	Example of an Image Produced by the Method Discussed .....	65
Fig. 3.3.1	A 3x3 Neighborhood About a Pixel (x,y) in a 256x256 Image .....	68
Fig. 3.3.2	Gray-Level Transformation Function for a 1x1 Sub-Image .....	69
Fig. 3.3.3	A 3x3 Sub-Image .....	72
Fig. 3.3.4	Procedure for Detecting Variations in Gray-level in an Image .....	73
Fig. 3.3.5	Image Pixel Locations and Coefficients of Sub-Image .....	74
Fig. 3.3.6	Local Image Enhancement Example .....	77
Fig. 3.3.7	Neighborhood Averaging Function .....	79
Fig. 3.3.8	Example of a Median Filtering Operation .....	80
Fig. 3.3.9	Example of Low-Pass Filtering .....	82
Fig. 3.3.10	Density Profile .....	83
Fig. 3.3.11	Average Density Profile .....	84
Fig. 3.3.12	An Example of Histogram Plot .....	86
Fig. 3.3.13	Contour Maps .....	87
Fig. 3.3.14	Saturation Front Example .....	88
Fig. 3.3.15	Arithmetic Average .....	89
Fig. 3.3.16	An Example of 3D Plot .....	90
Fig. 3.3.17	Average Intensity of 3D Plot in Fig. 3.3.16 .....	91
Fig. 3.4.1	NMR Longitudinal Image .....	94
Fig. 3.4.2	Saturation Plot .....	95
Fig. 3.4.3	Contour Map for the NMR Image in Fig. 3.4.1 .....	97
Fig. 4.1.1	Core Holder .....	105
Fig. 4.1.2	Layout of Flow System .....	106
Fig. 4.1.3	Layout of NMR Flow Experiment .....	107
Fig. 4.2.1	Visualization of Pixel Intensity .....	113

## LIST OF FIGURES CONTINUED

	Page
Fig. 4.2.2	A 256x256 Image Averaged to a 3x3 Cell Image ..115
Fig. 4.2.3	NMR Image Used in Example .....117
Fig. 4.2.4	Average Intensities of Cells in Cross Sectional Area of a Core .....118
Fig. 4.2.5	Saturation Front .....119
Fig. 4.2.6a	Density Plot of the Average Saturation .....121
Fig. 4.2.6b	Histogram of the Saturation .....122
Fig. 4.2.7	Saturation Profile in a 3D Plot .....123
Fig. 4.3.1	Relative Permeability as a Function of Gray-level @ ( $S_{wi}=0.15$ ) .....135
Fig. 4.3.2	Relative Permeability as a Function of Gray-level @ ( $S_{wi}=0.20$ ) .....136
Fig. 4.3.3	Relative Permeability as a Function of Gray-level @ ( $S_{wi}=0.25$ ) .....137
Fig. 4.4.1	Fluid Distribution in a Rock Sample .....140
Fig. 4.4.2	NMR Image Showing the Distribution of Oil .....141
Fig. 4.4.3	NMR Image of a Core Saturated with Oil .....142
Fig. 4.4.4	Cross Sectional Image for a Core Flooded With Oil .....143
Fig. 4.4.5	Image of a Vertical Section for a Core Flooded With Oil .....144
Fig. 4.4.6	Image of a Horizontal Section for a Core Flooded With Oil .....145
Fig. 4.4.7	Oil Saturation Profiles .....146
Fig. 4.4.8	Longitudinal Saturation Profile .....148
Fig. 4.4.9	NMR Signal Across the Length of the Core .....149
Fig. 4.4.10	Third Degree Function of Saturation Distribution ..151
Fig. 4.4.11	3D Plot of Oil Saturation .....152
Fig. 4.4.12	Contour Map of the Horizontal Image .....153
Fig. B.1	Flow Chart for Algorithm 1 .....166

**LIST OF FIGURES CONTINUED**

	Page
Fig. B.2	Flow Chart for Algorithm 2.....167
Fig. B.3	Flow Chart for Algorithm 3.....168
Fig. B.4	Flow Chart for Algorithm 4.....169

## CHAPTER I INTRODUCTION

In recent years consideration of microscopic mechanisms of fluid flow in porous media have taken on greater significance. Visualization of the fluid flow has become an important subject in reservoir engineering. Although research is progressing rapidly in the area of petrophysics, many unanswered questions exist in connection with relative permeability, displacement phenomena, residual fluid saturations, flow structure, etc.; and further analytical mathematical formulations are seriously indicated. It is hoped that systematic investigations into the microscopic mechanisms connected with the behavior of fluids in porous media will shed some light on some of the problems that the technology encounters.

### 1.1 Visualization Mechanism

A limited number of experimental investigators have discussed the problem of visualizing the mechanism of flow structure. Nuss and Whiting<sup>1</sup> made studies on the pore-space geometry of sandstone and limestone by injecting cores with an inert plastic and leaching the solid matrices to leave behind plastic models of the pore spaces. Schaefer<sup>2</sup> traced pore spaces microscopically through length of limestone cores by cutting away thin sections from the exposed faces normal to the line of view.

In 1949 two projects were organized in which dynamic flow phenomena were examined microscopically to uncover microscopic mechanisms. One was set up at the Pennsylvania State College where Lowman observed heterogeneous fluid flow phenomena in capillaries.

---

This thesis follows the style of the *Journal of Petroleum Technology*.

The second was the American Petroleum Institute Research Project 47B at the University of Oklahoma where microscopic studies of dynamic fluid phenomena in synthetic porous matrices have been made by visual observation<sup>3</sup>.

## 1.2 NMR Research

High resolution Nuclear Magnetic Resonance (NMR) spectroscopy has been used for chemical analysis and the investigation of the physical properties of molecules in solution. The basic idea of the NMR system is to separate molecular species and groups on the basis of variation in the chemical shift which depends on the chemical structure of the material under experiment<sup>4</sup>. Petroleum hydrocarbons contain hydrogen, therefore a proton magnetic resonance technique can be used to determine the oil saturation in the pores of a rock. The NMR system can produce images of the molecules under investigation because the signals recorded are obtained directly from fluids contained in the pores of the rock<sup>5</sup>. This type of imaging technique is promising to be useful in petrophysics and reservoir engineering, because NMR can image the physical and chemical properties of porous rocks and the different fluid saturations contained within their pores. Those images can be taken within seconds at any spatial direction. The experiments can be performed at reservoir pressure and temperature.

Principles of the NMR are based on the fact that by varying the strength of a magnetic field, over the sample, the NMR signals will be affected and special information is impressed on those signals. The signal with the information attached to it is called FID (Free Induction Decay). The image is generated by creating a spatially varied magnetic field that results in a spatial distribution of NMR frequencies. Both the signals and the frequencies are correlated to the individual volume elements of the sample<sup>6</sup>. Most imaging techniques take advantage of the frequency of the NMR signal. A spatially inhomogeneous magnetic field is applied across the sample to introduce phase shifts. The spatially non-



uniform magnetic fields are created by switching spatial gradient coils on and off.

Nuclear Magnetic Resonance (NMR) imaging techniques can be used to measure changing fluid saturations and relative permeabilities in porous materials. The recorded signals are a measure of the volumes of fluids residing in the pore spaces. The relative changes of saturation distribution within a core can also be mapped as a function of both time and distance in the core sample.

### **1.3 Investigation Procedure**

The investigation procedure consists of three major parts: The first part is preparing the core sample and running the NMR experiment. Secondly, downloading and processing the NMR data produced. And finally, analyzing the images in terms of saturation changes.

Figure 1.3.1 is a diagram of the investigation procedure that was followed. The GECSI-II spectrometer is provided with a monitor to view the images during the experiment. NMR data can, however, be saved on a magnetic tape and can be used at a later time. Raw image files can also be downloaded and transformed into binary code to be able to process them. The noise level may be reduced by performing image enhancement on the files. Image processing functions, when applied to the NMR data, improve the quality of the image and enhance its features. Image analysis can then be carried out using both the statistical and graphical image processing routines.

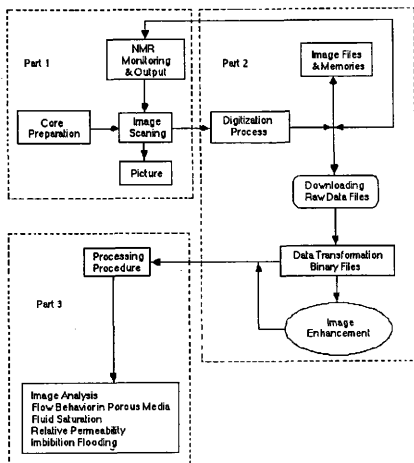


Figure 1.3.1  
Diagram of the Procedure of Flow Behavior Study Using NMR Techniques.

## **CHAPTER II**

### **NUCLEAR MAGNETIC RESONANCE**

### **THEORY AND EXPERIMENT**

The basic ideas of the theory of nuclear magnetic resonance and its experimental applications are explained in this chapter. The chapter starts in section 2.1 with a detailed introduction to the NMR theory. Section 2.2 is a discussion of the NMR signal in terms of relaxation times. An introduction to Fourier transform is also presented in this section. The basic hardware of the NMR spectrometer is discussed in section 2.3. Finally, the experimental applications of the NMR theory is discussed in section 2.4.

#### **2.1 NMR Theory**

Nuclear Magnetic Resonance theory is discussed in this section. Both the behavior of nuclei in a magnetic field, and the behavior of Magnetization are also explained in order to provide an understanding of the theory.

##### **2.1.1 Introduction**

Nuclear Magnetic Resonance is the phenomenon by which transitions between energy levels in the nuclei is produced by applying an electromagnetic field. A body with angular momentum can have a number of discrete spinning states<sup>7</sup>. Those states represent how fast or slow the body is spinning. Energy levels are characterized by a quantum numbers which are given symbols  $m$ ,  $l$ , or  $n$ .

NMR is possible because nuclei of many atoms possess magnetic moments and angular momentum<sup>8</sup>. A nuclear moment is just a fraction of the moment possessed by the electrons. When the magnetic moment interacts with a static magnetic field, the field tries to force the moment to

line up along the field just like a compass needle lines up with the earth's field. The significance of the angular momentum is that it makes the nuclei precess around the magnetic field when it experiences the torque due to the field acting on the moment. The result is that the nuclei precess about the field rather than oscillating in a plane like a compass needle.

### 2.1.2 The Behavior of Nuclei in a Magnetic Field

Nuclei of atoms have angular momentum, and therefore can spin about their axis. The different nuclei have different values of the spin quantum number,  $I$ . The spin of the nucleus produced a dipole. The magnetic moment of a dipole is the torque felt by the nuclei divided by the magnetic field strength<sup>9</sup>.

When a nucleus is placed in a magnetic field, a torque can act on the nucleus until it is aligned with the magnetic field around it. Energy states can be described by a quantum number called the *magnetic quantum number*,  $m$ , and it has value of  $I, I-1, I-2$ , but can not exceed  $-1$ . If  $I=1, m=0$  or  $-1$ .

The precession frequency of the moment is proportional to the gyromagnetic ratio,  $\gamma$  and the strength of the magnetic,  $H_0$ . Multiplying these two quantities will result in the Larmor velocity,  $\omega_0$  which is  $2\pi$  times the Larmor frequency,  $\nu_0$ .  $\gamma$  is the proportionality constant between the moment  $\mu_m$  and the angular momentum,  $p = \hbar\gamma$ ; so that:

$$\mu_m = \gamma\hbar \quad \dots \dots \dots (2.1.1)$$

Therefore, in a given magnetic field, the precession frequency is different for each distinct nucleus because each has a uniquely defined  $\gamma$ . For a typical nuclei used in NMR, the Larmor frequency falls in the range of a

few to a few hundred MHz in magnetic fields of commonly available magnets.

Nuclear moment precessing about a static magnetic field suffers no friction. It will precess forever while maintaining a fixed angle with respect to the magnetic field if left alone. Quantum mechanics requires that the orientation of a magnetic moment with respect to the field be quantized. The number of allowed orientations is  $2l+1$ , where  $l$  is the nuclear spin quantum number. Energy of a magnetic moment,  $\mu_m$  in a magnetic field,  $H_0$  is  $-\mu_m H_0$  so a positive moment will always want to line up parallel with the field.

A moment can undergo a transition to the higher energy state by receiving an appropriate amount of energy. A nucleus can also change energy levels as the frequency of the magnetic field changes. The angular momentum,  $P$  along the direction of the magnetic field is expressed as:

$$P = \frac{mh}{2\pi} = \frac{(l-1)h}{2\pi} \dots \dots \dots (2.1.2)$$

where  $h$  is Planck's constant. The magnetic moment,  $\mu_m$  is related to  $P$ :

$$\mu_m = \gamma P \dots \dots \dots (2.1.3)$$

where  $\gamma$  is the gyromagnetic ratio which is a characteristic for each nucleus. Substituting the expression of  $P$  into this equation results in a relationship between the moment and the magnetic quantum number, Thus:

$$\mu_m = \frac{\gamma m h}{2\pi} \dots \dots \dots (2.1.4)$$

Substituting  $\omega_0$  into the equations 2.1.1, 2.1.2 and 2.1.4 will result in a relationship between Larmor frequency and the angular velocity.

$$\omega_0 = \frac{2\pi\nu}{m} \dots \dots \dots (2.1.5)$$

The torque,  $\epsilon$  produced by the interaction between the magnetic field and the spinning nucleus is given by the product of the strength of the magnetic field  $H_0$  and the magnetic moment  $\mu_m$ . The produced torque acts in the opposite direction of the energy level. This relationship can be expressed as:

$$\epsilon = - mH_0 \dots \dots \dots (2.1.6)$$

This torque is equivalent to the energy produced by the magnetic field, and always tries to line up parallel with the magnetic field. Substituting equations 2.1.2, 2.1.3, and 2.1.4 into equation 2.1.6 will result in a relationship between torque and the magnetic quantum number,  $m$ .

$$\epsilon = - \frac{\gamma m h H_0}{2\pi} \dots \dots \dots (2.1.7)$$

This moment is parallel to the field, and can undergo a transition to a higher energy state by receiving an appropriate amount of energy. By changing energy states,  $m$  will change producing a change in  $\epsilon$ . The torque produced by the difference in energy levels can be given by:

$$\Delta\varepsilon = - \frac{\gamma\hbar H_0(m_2 - m_1)}{2\pi} \dots \dots \dots (2.1.8)$$

Electromagnetic radiation has different energy levels. The radio-frequency of the magnetic field can be adjusted to produce an amount of energy equal to the energy change in the nucleus. This will produce resonance, and the energy produced by the magnetic field is absorbed by the nuclei.

Electromagnetic radiation of frequency  $\nu$  has energy  $\Delta\varepsilon$  which can be represented as  $h\nu$ . Figure 2.1.1 shows the two energy levels of a proton and the difference in energy,  $\Delta\varepsilon$ . The change in energy level for both the magnet and the nucleus can be represented by the following two equations:

$$\Delta\varepsilon_m = h\nu \dots \dots \dots (2.1.8a)$$

$$\Delta\varepsilon_n = - \frac{\gamma\hbar H_0(m_2 - m_1)}{2\pi} \dots \dots \dots (2.1.8b)$$

Combining equation 2.1.8a and 2.1.8b with equation 2.1.1 will produce a relationship between frequency and energy level.

$$\omega_0 = -\gamma H_0 \dots \dots \dots (2.1.9)$$

The nucleus will not undergo the transition if the frequency of the radiation applied to induced transition is too high or too low. It is this fact of requiring exactly the right frequency to produce *resonance*, or in other words, to make the NMR very useful investigative tool.

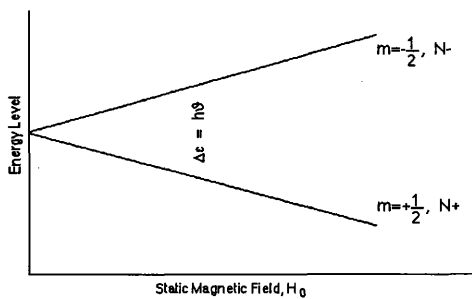


Figure 2.1.1  
Two Energy Levels



The frequency of the magnetic field,  $\nu$  must be determined to produce resonance for a particular element. For example, the frequency required for a Hydrogen nucleus to resonate in the magnetic field of 1.4 tesla is  $60 \times 10^6$  Hz. Since  $l=1/2$  for  $H^1$ ,  $m_2=1/2$  and  $m_1=-1/2$  (i.e.,  $m_2-m_1=1$ ).

The energy levels vary according to the Boltzman distribution when thermal equilibrium is established with the surroundings<sup>10</sup>. If the low energy level spins,  $N_+$  are in  $m=+1/2$  state and the high energy level spins,  $N_-$  are in  $m=-1/2$ , then:

$$\frac{N_+}{N_-} = \exp\left(\frac{\Delta E}{kT}\right) \dots \dots \dots (2.1.10)$$

Where  $K$  is the Boltzman constant, and  $T$  is the equilibrium temperature. At normal temperature of a magnetic field of a few kilogauss, there is a slight excess of population in the lower energy level. For protons, at room temperature in a field of 5,000 gauss;

$$\frac{N_+}{N_-} = 1 + 4 \times 10^{-6} \dots \dots \dots (2.1.11)$$

The energy difference for protons in the two levels is about 4.3 megacycle per 1000 gauss. Thus, the transition between the levels can be induced by applying a small ratio frequency field,  $H_1$  rotating in a plane perpendicular to the static field,  $H_0$ .

The nucleus has a magnetic moment and angular momentum. The magnetic moment interacts with the magnetic field,  $H_0$  and the magnetic field will force the moment to line up with the field. The moment would align along the direction of the magnetic field.

The nuclei have angular momentum and the effect is to force the nuclei and the magnetic moment to rotate about the field,  $H_0$ . The rotation velocity,  $\omega_0$  of the moment is determined by the gyromagnetic ratio of the nucleus,  $\gamma$  and the strength of the magnetic field. The direction of rotation is opposite to the direction of spin of the nucleus. The magnetic moment rotation is shown in Figure 2.1.2. The relationship between the velocity,  $\omega_0$  and the magnetic field,  $H_0$  can be presented by equation 2.1.9,  $\omega_0 = \gamma H_0$ . Where  $\omega_0$  is in radian units. It can, however, be divided by  $2\pi$  and change the units to Hz.

$$\nu = \frac{\omega_0}{2\pi} = -\frac{\gamma H_0}{2\pi} \quad \dots \dots \dots (2.1.12)$$

equations 2.1.5 and 2.1.12 are identical when  $m_2 - m_1 = 1$ .

### 2.1.3 Magnetization Behavior

Consider a sample in magnetic field at room temperature. All protons in the sample have the same positive moments and will line up with the field. Both temperature and the magnetic field alter the energy states of the protons. At room temperature, most of the protons are randomly distributed; some are parallel to the field while others are not, and their effects cancel. A large portion of these protons will line up and will provide magnetization,  $\bar{M}$  whose precession can be detected under certain conditions. The magnetization vector exists at equilibrium and is parallel to the field. Magnetization also obeys the Larmor relationship and precesses about any static magnetic field. Magnetization can relax back to thermal equilibrium by giving up quanta of energy to the surroundings if the magnetization is rotated away from the magnetic field. If a magnetic field rotating at Larmor frequency was applied in a plane

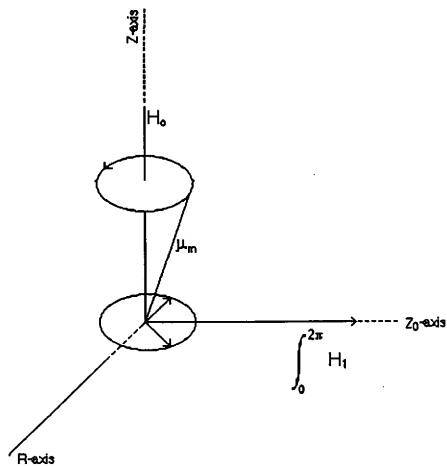


Figure 2.1.2  
Rotation of The Magnetic Moment About the Magnetic Field.

perpendicular to the static field, the magnetization will turn towards or away from the static field. Equations for both the effective magnetic field,  $\overline{H}_{\text{eff}}$  and magnetization,  $\partial\overline{M}/\partial t$  can be derived using vector analysis<sup>11</sup>.

Magnetization which is the change in magnetic moment with time, is a function of both magnetic moment in a sample and the magnetic field applied to the sample.

$$\frac{d\overline{M}}{dt} = \gamma\overline{M} \times \overline{H} \quad \dots \dots \dots (2.1.13)$$

Where  $\gamma$  is the gyromagnetic ratio defined as the moment divided by the angular momentum;

$$\gamma = \frac{\mu}{p} \quad \dots \dots \dots (2.1.14)$$

The Magnetization equation states that the rate of change of magnetization for a given nucleus having a specific  $\gamma$  is proportional to both the Magnetization and the magnetic field. The direction of change is perpendicular to both the magnetization and the field. The result s of this relationship is a precession of  $\overline{M}$  about  $\overline{H}_0$  at an angular velocity  $\gamma\overline{H}_0$ .  $\partial\overline{M}/\partial t$  of a vector  $\overline{M}$  moving with angular velocity  $\overline{\omega}$  can be expressed as:

$$\frac{\partial\overline{M}}{\partial t} = \frac{d\overline{M}}{dt} - (\overline{\omega} \times \overline{M}) \quad \dots \dots \dots (2.1.15)$$

Where  $\frac{d\bar{M}}{dt}$  is defined when there is no magnetic field applied. The time derivative of  $\bar{M}$  when a magnetic field is applied at a Larmor velocity  $\bar{\omega}$  is the same as that of no external magnetic field except for the substitution of a new field  $\bar{H}_{\text{eff}}$ ; so

$$\frac{\partial \bar{M}}{\partial t} = \gamma \bar{M} \times \left( \bar{H}_o + \frac{\bar{\omega}}{\gamma} \right) \dots \dots \dots (2.1.16)$$

$$\frac{\partial \bar{M}}{\partial t} = \gamma \bar{M} \times \bar{H}_{\text{eff}} \dots \dots \dots (2.1.17)$$

The effective magnetic field can be expressed as:

$$\bar{H}_{\text{eff}} = \bar{H}_o + \frac{\bar{\omega}}{\gamma} \dots \dots \dots (2.1.18)$$

If the rotating angular velocity  $\bar{\omega}$  is equal to the Larmor velocity  $\omega_o = -\gamma \bar{H}_o$ , the effective magnetic field will be zero; and the magnetization will be zero in the rotating frame.

$$\bar{H}_{\text{eff}} = \bar{H} - \frac{\gamma \bar{H}_o}{\gamma} = \bar{H}_o - \bar{H}_o = 0 \dots \dots \dots (2.1.19)$$

and

$$\frac{\partial \bar{M}}{\partial t} = 0 \dots \dots \dots (2.1.20)$$

So, the magnetization is static. But if we apply some external magnetic field  $\bar{H}_1$ , then:

$$\bar{H} = \bar{H}_0 + \bar{H}_1 \quad \dots \dots \dots (2.1.21)$$

and

$$\bar{H}_{\text{eff}} = \bar{H}_0 + \bar{H}_1 + \frac{\bar{\omega}}{\gamma} \quad \dots \dots \dots (2.1.22)$$

But at resonance,  $\bar{\omega} = -\gamma\bar{H}_0$ , thus

$$\bar{H}_{\text{eff}} = \bar{H}_1 \quad \dots \dots \dots (2.1.23)$$

This relationship states that only the external magnetic field is effective in the NMR experiment.

A pulse with a certain angle along  $H_1$  will act on the nuclei when exposing the sample to a magnetic field. The nuclei exchange energy with each other causing the magnetization to vary with time. This process is called the spin-spin relaxation,  $T_2$ . At the end of the pulse, the nuclei can also lose energy to the surroundings as they relax back to align themselves along their original position. This is called spin-lattice relaxation,  $T_1$ . Relaxation time will be explained in detail in a later section.

Once the pulse is tuned off, an exponential decay in signal (I) is observed as the nuclei relax. This decay is termed the Free Induction Decay or FID. FID can be expressed as a plot of signal intensity against time. It also can be expressed as signal intensity against frequency. This follows from the fact that signal intensity can be expressed as a function

of both frequency and time using Fourier transform.

A one dimensional signal is needed for NMR purposes. Figure 2.1.3 shows the transformation from signal as a function of time to an intensity as a function of frequency.

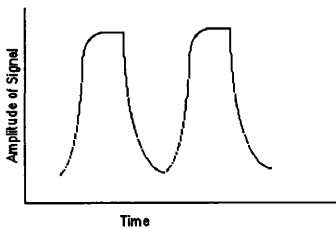
If the frequency of the applied electromagnetic field is different from resonance frequency of the nuclei, the nuclei will rotate, but the magnetization will get out of phase with magnetization on resonance. As a result, the FID will oscillate as the magnetization gets in and out of phase. The intensity of the signal will decrease with time as the signal intensity is lost by relaxation.

If there was two magnetization vectors, one at the magnetic field frequency and the other is rotating in the rotating frame slightly off the magnetic field frequency, there will be two signals, one in phase and the other changes phase as it rotates in the rotating frame. When applying Fourier transformation to the two signals, the two signals will be 180 degrees out of phase as in Figure 2.1.4.

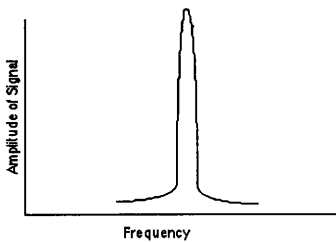
GECSI is provided with software to adjust the read-out of the spectrometer by phasing so that the magnitude of the two signals can be compared. The two signals, however, resonate at different frequencies. Since the frequency at which the nuclei resonate is determined by the properties of the molecules, the NMR can be used to distinguish between different nuclei.

#### **2.1.4 Chemical Shift**

The principle application of NMR is the determination of chemical shift. Same nuclei can resonate at different frequencies if they were in different environments or different chemical composition. The reason behind this fact is that the electron surrounding the nucleus after the



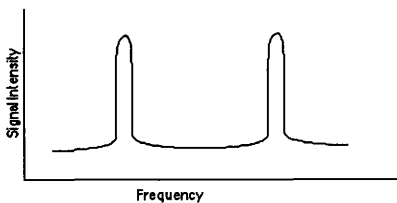
(a) Time Domain Signal



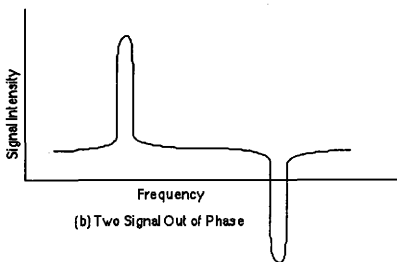
(b) Frequency Domain Signal

Figure 2.1.3  
Time and Frequency Domain Signals





(a) Two Signal In Phase



(b) Two Signal Out of Phase

Figure 2.1.4  
Phase Shifting Using FT

magnetic field experienced by it. The change in magnetic field is called a shielding factor. The shielding factor is responsible for the chemical shift.

The goal is to obtain separation of the molecular species and functional groups on the basis of variations in the chemical shift which depends on the local chemical bonding.

The chemical shift is due to the orbital effects of the nearby electrons. Electrons produce a small field when an electron or a molecule is placed in a static magnetic field. The direction and magnitude of this field depend on the electronic structure of the atom or molecule. The ability of the electrons to shield the nucleus depends in part on the direction of the magnetic field with respect to the electronic orbits. Thus, the chemical shift is a tensor quantity. The shift observed in liquids experiments is motional averages of the tensor components.

### **2.1.5 Detection of Elements by the NMR**

NMR is used to detect the elements of a solution by producing different signal type and amplitude for each element. Many factors influence the detection of elements by NMR. Some of the factors are:

- 1) The concentration of the element in the sample.
- 2) The value of the  $\Delta\varepsilon$  depends on  $H_0$  and  $\gamma$ ; so the field strength used and the characteristics of the nucleus are also important in detecting the element.

Nuclei with small values of gyromagnetic ratio,  $\gamma$  have small dipole moments and are difficult to detect.

## 2.2 Relaxation and Fourier Transform

In this section, We will explain simple concepts of both the Spin-Lattice relaxation and the spin-spin relaxation. A brief explanation of the way Fourier Transform work is also included.

### 2.2.1 Spin-Lattice Relaxation

A particle with a magnetic moment  $\bar{\mu}_m$  in a static magnetic field  $\bar{H}$  has two energy states separated by  $\Delta\epsilon = 2\pi H$ . A group of spin-1/2 nuclei placed in a magnetic field can distribute themselves between the two states so that the ratio of the number of spins in the upper energy states to that in the lower energy state is  $\exp[\Delta\epsilon / KT]$  at equilibrium; where T is the temperature and K is the Boltzman constant. There will be more spins in the lower energy state than in the upper state as a result of this magnetization, and the population difference will give rise to a magnetization,  $\bar{M}_0$ . The magnitude of the magnetization,  $\bar{M}_0$  depends on the field,  $\bar{H}$ , the temperature, T, The number of spins, N, the angular momentum,  $lh$ , and the gyromagnetic ratio,  $\gamma$ . This relationship is presented by Curie's Law as <sup>12</sup>:

$$M_0 = \frac{N\gamma^2 h^2 l(l+1) H}{3KT} \dots \dots \dots (2.2.1)$$

The orientation of the moments will be distributed equally between the two energy states when a sample is inserted into a field, . The amount  $2\mu H$  of energy is produced to turn the moment  $\bar{\mu}_m$  parallel to the field. A jump to a lower energy state requires a transfer of this energy to an external agent. The rate at which magnetization increases in a static field depends on the availability of an external agent to absorb the produced energy.

A spin in a high energy state can make a transition to the lower energy state by means of emission. Spin can jump to a lower energy state by emitting a photon. An external field usually acts as the agent that absorbs the energy. A time varying magnetic field which can interact with the nuclear magnetic moment is an example of such a field. Spin-lattice relaxation through magnetic transitions can be accomplished by different mechanisms. The mechanisms used are:

- 1) Dipole-dipole.
- 2) Scalar relaxation.
- 3) Spin rotation, and
- 4) Chemical shift relaxation.

The macroscopic magnetization obeys the Larmor relation. Magnetization precesses about any static magnetic field at a rate proportional to the field strength and the individual nuclear moment. The precession occurs with a constant cone angle in the absence of external work or friction. If magnetization is rotated away from the field, it can relax back to thermal equilibrium by giving up energy to the surroundings in multiple of  $h\theta$ . The surroundings which can absorb this energy are called the lattice. Those surroundings are usually paramagnetic impurities.

Those impurities are considered an important relaxation mechanism. Spin diffusion to paramagnetic impurities is an important mechanism, not only in solids, but in large molecules which exist in solutions. Both  $T_1$  and  $T_2$  relaxation rates due to the chemical shift are proportional to the square of the static field.

The interaction between the nuclear spin and the molecular magnetic moment arises from the angular momentum of the rotating molecule. When the molecule remains in a constant angular momentum state, its electronic structure produces a constant electric current and this would not lead to relaxation but collisions with other molecules can

cause fluctuations of the angular momentum. This collision can cause relaxation. This coupling is described in terms of spin rotating tensor C. The spin-lattice relaxation rate is

$$\frac{1}{T} = \left( \frac{2IKT}{3h^2} \right) (2\pi C_o)^2 \tau_j \quad \dots \dots \dots (2.2.2)$$

where  $C_o/3$  is the average of the principle values of the tensor C in units of frequency, I is the moment of inertia of the molecule about the appropriate axis, and  $\tau_j$  is the angular momentum correlation time.

Relaxation times for solids are usually short. It is often not possible to see an FID for them. This fact enables only the liquids contained in a rock and not the material of the rock to be seen. The molecular motion of solids controlling the relaxation times at higher temperatures slow down and the relaxations of the fluids in the solids usually takes over At low temperature.

Nuclear spin-lattice relaxation processes depend on the existence of molecular motion to generates varying magnetic field. This will result in valuable information.

## 2.2.2 Spin-Lattice Relaxation Measurements

Spin-lattice relaxation behavior is usually described as exponential. The total magnetization recovered during any time can be expressed as a function of the exponential of the relaxation time <sup>13</sup>.

$$M(t) = M_o \left[ 1 - \exp\left(\frac{-t}{T_1}\right) \right] \quad \dots \dots \dots (2.2.3)$$

The lattice relaxation time,  $T_1$  is defined only for exponential processes. The actual process of relaxation may not be exponential.

There are several choices to measure  $T_1$  by a  $\pi$ - $\pi/2$  sequence for which magnetization obeys the relationship above. One method is to measure  $\frac{M(t)}{M_0}$  and plot  $1 - \frac{M(t)}{M_0}$  against time,  $t$  on a semilog plot. The relaxation equation can be written as:

$$1 - \frac{M(t)}{M_0} = 2 \exp\left(-\frac{t}{T_1}\right) \quad \dots \dots \dots (2.2.4)$$

Figure 2.2.1 is a plot of this relationship showing the magnetization as a function of time.

The usual method of determining the spin lattice relaxation time is to measure  $M(t)$  at various values of  $t$  and fit them to the equation 2.2.4 above by either a semilog plot or a computer.  $M_0$  must be determined by accurately in order to get a correct value of  $T_1$ .

### 2.2.3 Spin-Spin Relaxation

Spin-spin relaxation is the process in which the magnetization in the  $R-Z_0$  plane perpendicular to the static magnetic field, decays. Spin-spin relaxation is represented by the symbol  $T_2$ . Both  $T_2$  and  $T_1$  contain different information when they are not equal.  $T_1$  and  $T_2$  are usually different for solids. This also can happen quite often in liquids as well. This should enable us to obtain additional information about the fluids in the rock <sup>14</sup>.

Spin-spin relaxation has a characteristic time  $T_2$ .  $T_2$  is the time constant for the decay of the precessing  $R-Z_0$  component of the magnetization following a disturbance. The relaxation is commonly described by an exponential function. The rate of the function is characterize the reciprocal of the first order rate relaxation time constant.

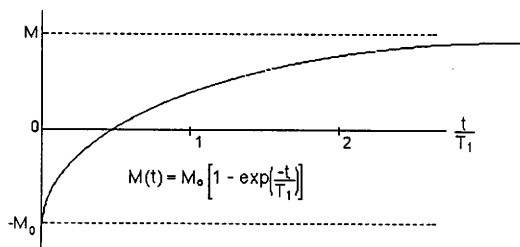


Figure 2.2.1  
Magnetization as a Function of Time.

Even though the relaxation process may appear as an exponential process, it is not similar to radioactive decay. The process is generally not first order.

The rate of relaxation is commonly described by an exponential function and can be characterized by the reciprocal of the first order rate relaxation time constant.  $1/T_1$  and  $1/T_2$  have units of angular velocity (radian/second) and the NMR spectral display is in units of frequency, so the relaxation times need to be transformed into Hz. Even though the relaxation process may appear as an exponential process, it is not similar to radioactive decay. The process is generally not first order. When molecular motions are very fast, as in non-viscous liquids,  $T_1 = T_2$  for most interactions and  $T_2$  offers no additional information. However, generally  $T_1 \gg T_2$  and then  $T_2$  does offer additional information.

#### 2.2.4 Fourier Transform

Any representation in the time domain can be transformed into an equivalent representation in the frequency domain and vice versa using Fourier transformation. For example, consider a sine wave in the time domain shown in Figure 2.2.2(a). An alternative representation of this sine wave would be a spectrum of amplitude as a function of frequency which represents a histogram of frequencies as shown in Figure 2.2.2(b). These two representations, amplitude vs. time and amplitude vs. frequency, both contain the same information. One representation can be transformed into the other by a mathematical technique called Fourier transform. FT is represented by <sup>15</sup> :

$$A(t) = \frac{1}{2\pi} \int_{-\infty}^{\infty} A(\omega) e^{i\omega t} d\omega \dots \dots \dots (2.2.5)$$

$$A(\omega) = \int_{-\infty}^{\infty} A(t) e^{-i\omega t} dt \dots \dots \dots (2.2.6)$$



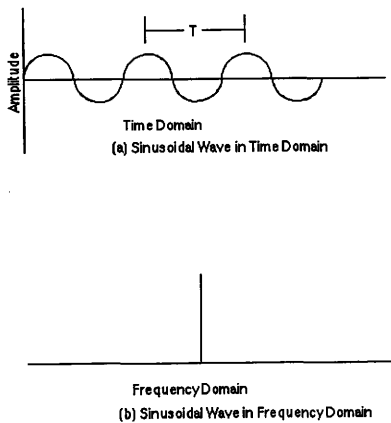


Figure 2.2.2  
Sine Wave Transformation Using FT

The frequency is multiplied by a sinusoidal wave of unit amplitude,  $e^{-i\omega t}$ , and this product is added over all times at frequency,  $\omega$  in the transformation from time to frequency domain. The translation from frequency to time space is the inverse of this process.

Assume a spectrum is a representation in the frequency domain. The individual lines represent the sinusoidal waves occurring at those frequencies. Consider a frequency domain spectrum consisting of two lines with finite width. Each line would correspond to an exponentially decaying sinusoidal wave. The result is a very complex pattern called the free induction decay (FID) which is what is recorded in an actual experiment if all these individually decaying sinusoidal waves are summed.. The Fourier transform yields the spectrum corresponding to such an FID.

Consider a benzene molecule with only chemically equivalent protons. This molecule will result in a large magnetization vector in equilibrium with the applied field. A  $90^\circ$  pulse applied at a time  $t=0$  will rotate this magnetization into the R-Z<sub>0</sub> plane at which point it will precess in time at the Larmor frequency and will decay exponentially with the time constant,  $T_2^*$ . A voltage will be induced in the coil mounted in the R-Z<sub>0</sub> plane. This voltage is a decaying sinusoidal. If this signal was sent to an analog-to-digital converter, and the digitized decaying sinusoidal wave is Fourier transformed in digital computer, the output would be the NMR spectrum of the molecule as shown in Figure 2.2.3.

If the sample contained molecules with more than one chemically different groups of protons such as ethyle alcohol, the  $90^\circ$  pulse would rotate all contributions to the magnetization by  $90^\circ$  and all of the components would be precessing in the R-Z<sub>0</sub> plane with their own Larmor frequency. The resulting FID is a very complex pattern of different sinusoidal waves all starting with the same phase. The output would be the spectrum of this molecule if this complex signal was digitized and Fourier transform.

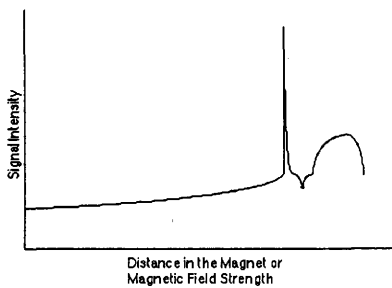


Figure 2.2.3  
NMR Spectrum

## 2.3 NMR Components

In the following section, we consider, in general terms, the actual hardware which make up NMR spectrometers.

### 2.3.1 NMR Types

There are three types of NMR spectrometer. Pulse, Pulse Fourier Transform, and continuous wave spectrometer<sup>16</sup>. The pulse spectrometer records only signal intensity as a function of time and is not used anymore. The change of frequency with time can be recorded by the continuous wave spectrometer. This type of spectrometer is inexpensive and has wide spread applications in Organic Chemistry for studying protons. The continuous spectrometer is not important in the case of hydrocarbon flow in porous media.

The pulse Fourier Transform NMR Spectrometer is the applicable to the case of studying fluid flow. It produces time spectrum and then Fourier transform them to frequency domain. Spectra of frequency against time is recorded only. The frequency of irradiation of the sample is changed more rapidly than the rate at which the nuclei can relax.

Usually a pulse NMR is used to give a spectrum in the time domain, and Fourier transformation is applied to the frequency domain. NMR spectrometer is capable of undertaking experiments in both time and frequency domains.

An NMR spectrometer consists of a magnet, a frequency source, a transmitter, a probe, a detector, and a computer for Fourier transformation. A decoupler is also used for irradiating one type of nucleus while observing the other. In NMR, the sample is exposed to a magnetic field,  $H_0$ . The applied irradiation field has an angular velocity  $\omega_0 = \gamma H_0$  and a frequency  $\nu = \omega_0/2\pi$ . The output from the sample is small

and it needs to be spectrometer consists of three major parts: Frequency transmitter, sample placed in a magnet, and a receiver to amplify and detect the signals coming from the sample. A computer receives and analyzes the signals. Figure 2.3.1 is a diagram of the major components of the NMR.

### **2.3.2 Transmitter**

The transmitter consists of a frequency source and amplifiers to boost the frequency signals to the desired level. An oscillator is used to turn the frequency on and off since NMR requires that the irradiation must be transformed into pulses. A diagram of the oscillator and its performance is shown in Figure 2.3.2.

### **2.3.3 Receiver**

NMR receivers consist of amplifier stages to multiply the irradiation signals large enough to be detected. The detector passes only the signals carrying the desired information. The detected signals are usually further amplified in order that the signals will be the right size for the digitizer as shown in Figure 2.3.3.

The primary job of the receiver is to amplify and detect signals without introducing distortion or additional electrical noise. The noise is usually generated by both the transmitter and the receiver, the NMR coils, the sample, and other external sources such as electrical noise in the laboratory.

The tuner is set to limit the range of frequencies admitted to the receiving system to eliminate the noise. This process is called a narrow banding. Narrow banding is usually accomplished by mixers (Phase Sensitive Detectors). Each of the mixers forms the sum and difference of the input frequencies. The amplifier is tuned to  $\omega_1$  and all other frequencies will be disregarded. The result is that the signal being amplified by the amplifier is always  $\omega_1$  regardless of the Larmor frequency

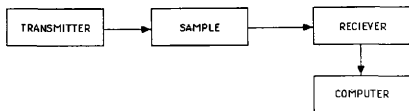


Figure 2.3.1  
Major NMR Components

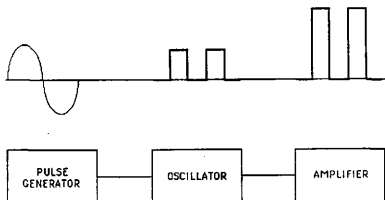


Figure 2.3.2  
Transmitter



Figure 2.3.3  
Receiver

$\omega_L$ . So  $\omega_L$  can be changed without affecting the operation of the system. Assuming that a sample will resonate at 29 MHz as shown in Figure 2.3.4. A local oscillator frequency of 129 MHz has to be applied in order to get this frequency from the 100 MHz.

### 2.3.4 Magnets

Magnets are essential to all magnetic resonance experiments. There are four kinds of magnets to consider for use in magnetic resonance: Air-core electromagnet, A permanent magnet, An iron-core electromagnet, or a superconducting magnet. Although the superconducting and the permanent magnets are being used extensively, The electromagnets still constitute the majority of magnets for NMR research. The magnetic field intensity depends on both the permeability of the iron in the magnet and the electrical current. Well thermostated room with well-regulated cooling water is usually used to maintain stability.

Electromagnets rely on electric currents to produce the field. A great deal of heat is generated in this process. The laboratory environment, for that reason, must be able to exhaust this heat. The magnet usually contains a space for the sample to be placed in. The larger the sample space, the smaller the maximum field strength.

### 2.3.5 Data Acquisition System

The data obtained from the experiment must be digitized in order to perform Fourier transformation. The digitization process can be classified based on the time it takes to perform the operation. In high resolution NMR, the maximum digitizing rate used is tens of KHz. If an FID lasts for 2 seconds and is digitized at 10 KHz, the total number of points recorded with single precision of 20,000. Figure 2.3.5 shows a picture of an NMR Spectroscopy.

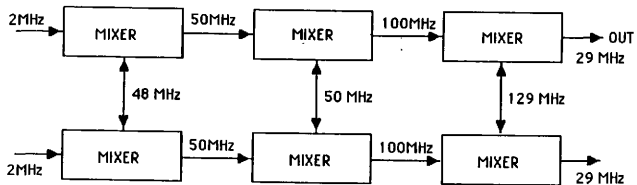


Figure 2.3.4  
The Operation of Phase Sensitive Detectors



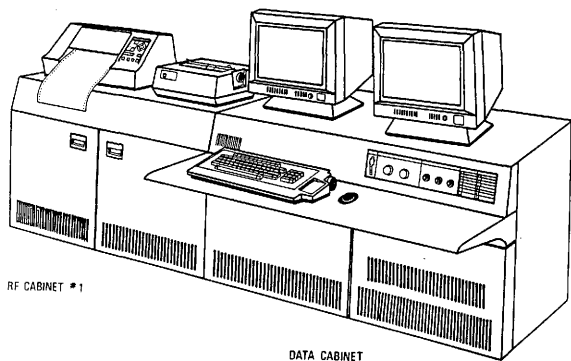


Figure 2.3.5  
NMR Spectroscopy (from Reference 16)

## 2.4 NMR Experiment

In this section, we give a qualitative description of the way the NMR theory works in an actual NMR experiment.

### 2.4.1 Applications of NMR Theory

In NMR experiments, an intense rf pulse with an amplitude of  $H_1$  is applied to the sample. At resonance, the effective magnetic field should equal the applied magnetic field along the rotating axis R<sup>17</sup>.

$$\bar{H}_e = \bar{H}_1 \quad \dots \dots \dots (2.4.1)$$

The Magnetization,  $\bar{M}$  will rotate about  $H_1$  in the plane  $Z-Z_0$  with an angular velocity  $\gamma\bar{H}_1$ . Figure 2.4.1 is a 3D Cartesian plot showing the spatial relationship between the magnetization and the applied magnetic field. The angle between the magnetization and the Z direction is changing with time,  $t$ , and it can be expressed as

$$\theta = \gamma\bar{H}_1 t \quad \dots \dots \dots (2.4.2)$$

If the magnetic field produced a rotation of 90°, this magnetic field will be called a 90° pulse. If the magnetic field was applied for four times as long, it will be called a 360° pulse.

In the case of a 90° pulse, the magnetization,  $\bar{M}_0$  along the axis  $Z_0$  will decay in time as the system comes back to equilibrium. The decay in

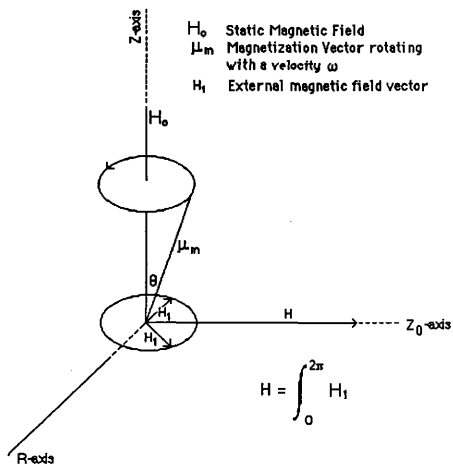


Figure 2.4.1  
Rotation of The Magnetic Moment About the Magnetic Field.

the  $R-Z_0$  will be exponential with the time constant  $T_2$  which is known as the spin-spin relaxation time. The output of this pulse will be a sinusoidal wave whose amplitude decays at a rate proportional to the exponential of  $T_2$ .

$$M_{\Omega} = \exp\left(\frac{-t}{T_2}\right) \dots \dots \dots (2.4.3)$$

The magnetization will re-establish itself along the Z direction in equilibrium with the applied field because of the spine-lattice relaxation time,  $T_1$ . The recovered magnetization can be expressed as a function of both the initial magnetization and the spin-lattice relaxation time.

$$M_z = M_0 \left[ 1 - \exp\left(\frac{-t}{T_1}\right) \right] \dots \dots \dots (2.4.4)$$

The decay rate in the  $R-Z_0$  plane is usually larger than the recovery rate along the Z-axis.

$$M_{\Omega} > M_z \dots \dots \dots (2.4.5)$$

Only magnetization in the  $R-Z_0$  plane is detected by the NMR coil. The magnetization along the Z-axis is not detectable until it is rotated away from the Z-axis. A second pulse will be necessary to measure the spin-lattice relaxation time,  $T_1$ .

The decay rate constant in the  $R-Z_0$  plane;  $1 / T_2$  is a function of the recovery rate along the Z-axis. The relaxation rate can be approximated by:

$$\frac{1}{T_2} = \frac{1}{2T_1} + \frac{1}{T_2} + \gamma\Delta H_0 \dots \dots \dots (2.4.6)$$

Where  $1/T_2$  is the decay rate constant produced by the mechanism which disperses magnetization in the R-Z<sub>0</sub> plane.

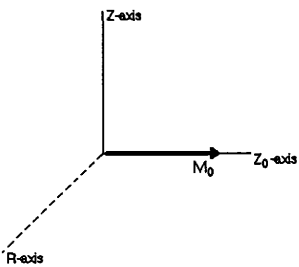
Consider a sample placed between the poles of an electromagnet. Different parts of the sample, in any real magnet, experience different fields as a result of the magnet inhomogeneity<sup>18</sup>. In NMR spectroscopy it is important to minimize this inhomogeneity in the applied static field for maximizing resolution. The required homogeneity varies widely depending on the experiment.

The magnetization, with a 90° pulse applied to a sample, will be rotated in a short time if the pulse is very intense in the inhomogeneous magnetic field. The magnetic amplitude will decrease shortly due to the field inhomogeneity. The total magnetization vector is the sum of smaller magnetization vectors each arising from a small volume experiencing a homogeneous field. Each of these components of the magnetization will precess with its own Larmor frequency after a 90° pulse. The different contributions of the magnetization will get out of phase with each other.

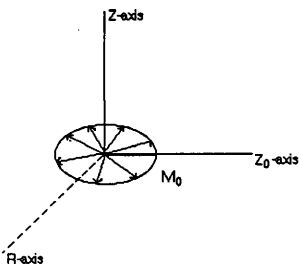
The FID will have a null or a minimum signal at successive 180° intervals. It is important to choose the first minimum signal. A 360° pulse is easily detected since half of it is a 180° pulse that results in a zero FID. One half a 520° pulse is a 270° and is indicated by an inverted signal.

Figure 2.4.2 shows that at time, t=0, magnetization,  $\overline{M}_0$  is along the Z<sub>0</sub>-axis. Shortly after t=0 and because of the inhomogeneity, magnetization vectors will form. The intensity and direction of these magnetization vectors is controlled by the relationship:

$$\theta = \gamma H_1 t$$



(a) Magnetization at time = 0



(b) Magnetization at Time &gt; 0

Figure 2.4.2  
Magnetization Behavior

The direction of the magnetization vectors is a function of both time and the magnetic field applied. As a result, some of the vectors will start getting ahead of the average magnetization and some starts getting behind. The result is that the net magnetization along the  $Z_0$ -axis decays to zero as the magnetization vectors sweep the  $R$ - $Z_0$  plane. The coil in the  $R$ - $Z_0$  plane will pickup the voltage induced. The voltage will decay as the vectors sweep out the  $R$ - $Z_0$  plane. This signal following the pulse is an FID and is shown in Figure 2.4.3.

$T_2$  is the time constant which describes the decay of magnetization in the  $R$ - $Z_0$  plane. This relaxation time which is characteristic of the magnetization decay without any field inhomogeneity effects is the spin-spin relaxation time.  $T_2$ ,  $T_2^*$ , and Larmor speed  $\gamma\Delta H_0$  are related by:

$$\frac{1}{T_2^*} = \frac{1}{2T_1} + \frac{1}{T_2} + \gamma\Delta H_0$$

If the magnetic field inhomogeneity is improved,  $T_2^*$  will increase until it equals  $T_2$ .

The spin-spin relaxation time does not involve any exchange of energy with the surroundings. The spin-lattice relaxation, however, depends on an outside agent accepting energy from the spin system so that the spin system can relax towards thermal equilibrium. The lattice can be of any form such as molecular rotation, diffusion, or lattice vibration.

## 2.4.2 Spectroscopy Experiments

High resolution NMR spectroscopy has been for chemical analysis as well as for the study of the physical properties and behavior of molecules in both solids and solutions. The experiments of this study were performed on a CSI-II spectrometer which is similar to the

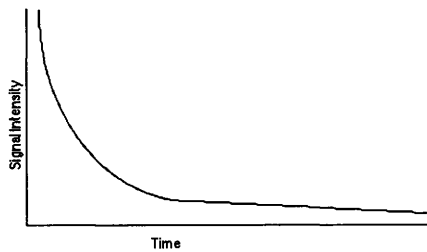


Figure 2.4.3  
Free Induction Decay (FID)



conventional high resolution NMR spectrometer, and is designed by the General Electric Company.

Several steps need to be performed before starting the experiment. These steps are:

- 1) Selecting the desired pulse sequence.
- 2) Preparing the sample, and placing it with the coil in the appropriate position in the magnet.
- 3) Tuning the surface coil.
- 4) Shimming the magnet.

Both the sample and the surface coil must be placed in the magnet in a position where the magnetic field is most homogeneous. This region is the intersection of the vertical and the horizontal planes of the magnetic field. It is essential for the normal to the plane of the surface coil to be perpendicular to the axis of the magnet.

The surface coil can observe signals twice the coil diameter in depth. Both the magnet and the coils of the CSI-II must be shielded to reduce the noise induction and ensure accurate results. It is necessary to tune the surface coil so that it resonate at the exact center frequency of the desired nucleus. The CSI-II spectrometer is provided with a computer command and monitor display to perform tuning.

The NMR frequency depends directly on the the magnetic field. Any variations in the magnetic field over the observed sample will result in broadening of the NMR lines, leading to a reduction in resolution and decrease in peak height. The magnetic field may be adjusted to correct for small distortions and to obtain the best possible homogeneity over the surface area of the sample. This process is called *shimming*. On the CSI-II, there are 14 variables involved in shimming the coils. Each variable is adjusted to correct a specified field distortion. Shimming can be performed easily using the shimming program incorporated in the GEMCSI software.

### **2.4.3 Experimental Runs**

Again, before running the experiment, the sample must be correctly positioned in the magnet, the surface coil has to be tuned, and the magnet needs to be shimmed. The experimental parameters such as pulse length, pulse height, and delay time need to be selected. Pulse experiment described above is available in the CSI-II System Pulse Sequence Library. The operator can call up this file and adjust the experimental parameters in the file. Once the parameters are adjusted for the the experiment, the Macro can be run.

### **2.4.4 Signal Processing**

When running the experiment, a number of FID s will be collected and stored in a memory block. A Fourier transformation is then need to be performed on the data to be able to display the spectrum. An example of the spectrum is shown in Figure 2.4.4 The spectra needs to be phased since the FT provides both the real and imaginary cosine and sine terms of the transformation. Phasing will allow one part of the spectrum to be phase-shifted with respect to the other to obtain the desired spectrum, which is shown in Figure 2.4.5.

### **2.4.5 Preliminary Experimentation**

The sample and a coil are placed in the magnetic field of the magnet. The rf magnetic field generated in the coil must be perpendicular to the static field. Magnetization will point along the magnetic field.

The sample is placed in the spectrometer and the frequency range and the optimum length of pulse are selected. The delay between the individual pulses is then selected from the knowledge of the relaxation time,  $T_1$  of the nucleus to be observed. The number of scans to be completed is then selected. The experimental conditions are then



**Figure 2.4.4**  
NMR Signal Before Correction

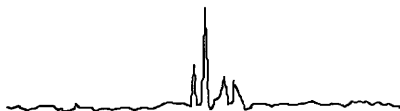


**Figure 2.4.5**  
NMR Signal After Correction

changed and the experiment has to be performed again. This procedure may be replicated several times. These experiments are necessary for measurements of relaxation time. After this preliminary experimentations, the spectrometer can be started and the computer will carry out the time events pre-programmed into its memory. The Fourier transformation data manipulation are then done.

#### **2.4.6 Laboratory Experiment**

A water wet dolomite core of 2 5/8" diameter and 5 7/8" long was used in this study. Since oil and water give ambiguous  $^1\text{H}$  NMR response,  $\text{D}_2\text{O}$  was used instead of water to obtain  $^1\text{H}$  response for oil only. The sample used had 27.29% porosity and 4.41 md permeability. A detailed setup of the laboratory experiment is discussed in section 4.1.

## **CHAPTER III NUCLEAR MAGNETIC RESONANCE DATA PROCESSING**

In this chapter, NMR data processing, the processing procedure of the NMR data files are discussed. The discussion is divided into two parts: First, the transformation of the data, which includes downloading, equalization and converting to binary code. The other part is applying the image processing function to analyze the NMR images. Section 3.1 is an introduction to image processing and the available image processing software. Data transformation is discussed in section 3.2. Section 3.3 contains a brief discussion of the processing functions that were used in this research. And section 3.4 contains a summary of image processing in terms of fluid flow.

### **3.1 Introduction**

High resolution images can provide useful information for detailed interpretation of features. Although the images contain useful information, the petroleum literature lacks imaging techniques in the study of fluid in porous media.

#### **3.1.1 Pattern Analysis**

Both statistical and structural approaches are used for treating pattern recognition. Statistical methods require sample databases. Structural methods try to construct a description of the image by constructing spatial relations between objects rather than considering the properties of a particular pixel<sup>19</sup>. Figure 3.1.1 is a diagram of the difference between the statistical methods and the structural methods.

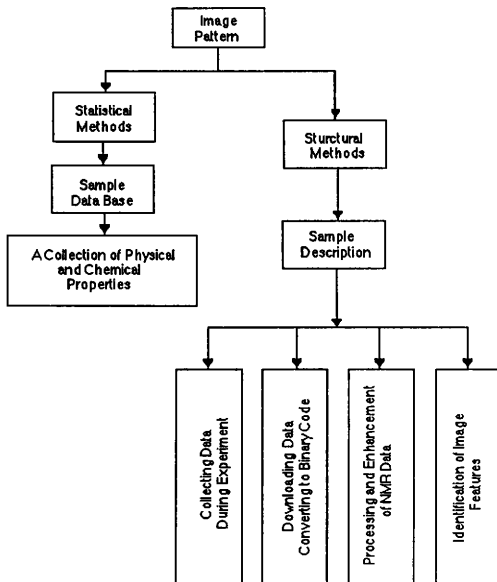


Figure 3.1.1  
Statistical & Structural Methods

Structural methods were chosen to accomplish the current research. Implementation was conducted in four steps. The first step involves collecting the data during the experiment. Next the data is downloaded to a personal computer. Third, the raw NMR data is processed to binary format. Lastly, image processing routines are used to identify the image features. While structural methods are able to use spatial relationships between objects, they also require good quality data.

A particular area in the pattern involves the recognition of image textures or patterns. Recognition of the image texture may simplify pattern recognition. Methodologies for the analysis of textures also fall into two broad categories: Statistical and structural. Statistical approaches to texture analysis include features based on the Fourier power spectrum, first order statistics of gray level differences, and second order gray scale statistics. All statistical methods require the definition of a unit that quantifies texture features.

Image texture is the disposition of the particles or members of a body or substance. A brick wall or a checkerboard are examples of image texture.

Computer interpretation of images is desirable for various reasons. First, they can focus attention on important matters and complete the details without human intervention. Second, computers do not tolerate imprecision or vagueness. Computers force us to take a critical look at our methods of interpretation. Third, computer models can be used to develop new methods for image interpretations.

### **3.1.2 NMR Data**

Computer systems drive the imaging process as well as display and record the proton resonance signals derived from a particular study. Huge volumes of raw data must be transformed to usable pieces of information for further analysis. Most NMR systems currently use some

type of rather expensive interactive work-stations, i.e. such as a Sun, for data manipulation and analysis.

The goal of this part of the study was to transfer the raw NMR saturation data files and process them using a PC or a Macintosh. This discussion is based on the GECSI-II Spectroscopy and Imaging System which has enough hardware to show a two-dimensional image of the saturation in any cross section. However, the system is not provided with software to process those images. Many public domain digital image processing programs are available. The programs generate image from various data sets, analyze, and animate, those images, create color maps, and present the results in a manner that is easy to understand.

Raw NMR data files are divided into 256X256 matrices of positive even digits. Initially, the files need to be downloaded to be used on a Macintosh. A program was developed to reduce the noise level of the image, to reformat the data to reduce the storage area needed for each file, and to convert the raw NMR data into file formats that can be read by any image processing program. The program takes advantage of the fact that the raw data files contain only positive even integers, by dividing each number by 2. Storage requirements are reduced from 4 bytes per pixel to 2 bytes. The maximum noise level is used as the start of the good data needed for the image. The data is then divided by 256 and a color ranging from 0 to 256 is assigned to each pixel which is then saved as binary data.

In-house developed functions along with public domain image processing programs were used to analyze the saturation data obtained from NMR experiments. Statistical routines were also used to obtain quantitative meaning of the images. Flow visualization was made possible by running a movie of images taken at different times. Visualization of the fluid distribution can be related to values obtained from the statistical routines to produce better understanding of the flow pattern.



## **3.2 NMR Data Transformation**

This section provides a summary of Histogram Equalization method used to reduce the noise level in the NMR data. The new method which utilizes a Macintosh II system to process the NMR data is discussed.

### **3.2.1 New Method**

A technique coupling public domain image processing programs with in-house programs for downloading and interpreting NMR data has been developed. The new method permits a PC or Macintosh II computer system to be used in place of the more sophisticated and expensive graphics work stations.

Raw NMR data files are downloaded via a parallel to serial link as 256x256 matrices of positive, even integers. In-house developed C Programs are used to convert the text files to binary data to reduce both storage requirements and image noise level<sup>20-22</sup>. An interactive portion of the program permits the operator to choose the level where the good data starts. The good data are then extracted and processed into colored images.

The extracted data is divided by 256 and a color table ranging from 0 to 255 is arranged. The end points are quantified by measuring these saturation values during the experimental run. The data is stored in binary form once a color has been assigned to each pixel. The process of converting the NMR files to binary files and assigning colors to the pixels takes 90-120 seconds of computer time. This process produces images with sufficiently good resolution to show saturation fronts and to distinguish features within the image.

### 3.2.2 Experimental Data

The data is collected for each image during the experiment in a file A.DAT which has a resolution of 256. This data is expressed as a plot of signal intensity against time. A Fourier transform is carried out with respect to one dimension and the results are stored in file A1.DAT. The second step is to transpose the resulting matrix. This operation interchanges the rows and columns of the matrix and stores the results in file A2.DAT. The second Fourier transform is performed on this data file and the results are placed in file A3.DAT. The final operation is to store the processed data in image file A3.IMG. These procedures are standard two-dimensional Fourier transform (2DFT) data processing steps which transform the signal intensity from time domain to frequency domain.

All data are collected in a temporary default file, named A.DAT, and processed to give an image data file A3.DAT. The data, however, must be saved under a different file name for use at a later time. Failure to rename the file after processing will result in the file being overwritten.

The raw NMR data files, now, contain 256x256 matrices of positive even integers. Figure 3.2.1 shows the data in an NMR raw image file. As shown in the figure, the data contains 256x256 positive even integers. The integers at the borders are small compared to the ones in the center. The data in the center (Three digit integers in Figure 3.2.1) is the good data that is processed to produce the image. The data at the borders is not useful and represents noise. The data is downloaded to be used on a Macintosh. Figure 3.2.2 shows an example of a data file after downloading. All necessary information such as the name and the size of the data file are included within the data file.

### 3.2.3 Histogram Equalization

A description of the appearance of an image can be provided by a

```

82 66 24 44 66 78 78 88 22 24 42 56 98 12 06 44 46 66 68
56 98 12 06 44 46 66 68 12 12 44 56 66 22 06 22 22 22 46
66 24 44 66 78 78 88 22 24 42 56 98 12 66 68 12 12 44 56
66 68 12 12 44 56 66 22 06 22 22 22 46 06 44 46 66 68 12
12 14 22 26 34 46 56 66 78 68 98 46 56 20 10 30 70 90 20
46 56 66 78 68 98 46 56 20 10 30 70 90 20 82 66 24 44 78
234 238 122 100 120 150 134 122 128 142 154 132 444 446 444 498 500 100 12
166 334 546 556 788 998 888 778 668 444 444 446 556 778 888 778 676 556 55
178 568 566 556 346 788 566 344 324 334 232 122 134 456 788 444 442 122 55
178 668 444 444 446 556 778 888 778 676 556 556 222 122 778 668 444 444 44
188 778 676 556 788 998 888 778 668 444 444 446 556 778 888 778 676 556 55
234 334 346 456 678 568 566 556 346 788 566 344 324 334 232 122 134 456 78
156 788 998 888 778 668 444 444 446 556 778 888 778 676 556 998 888 778 66
146 556 778 556 788 998 888 778 668 444 444 446 228 388 346 734 654 542 44
158 676 556 788 998 888 778 668 444 444 446 556 778 888 778 676 556 556 55
144 446 556 778 888 778 676 556 556 222 122 778 668 444 444 444 444 446 22
134 654 778 676 556 788 998 888 778 668 444 444 446 556 778 888 346 788 56
334 232 122 234 334 346 456 678 568 566 556 346 788 566 344 324 334 232 12
788 166 334 546 556 788 998 888 778 668 444 444 446 556 778 556 778 888 72
78 78 88 22 24 42 56 98 12 66 68 12 12 44 56 78 12 22 22
06 44 46 66 68 12 12 22 56 66 78 68 98 46 56 20 10 30 70
22 12 68 12 12 44 56 66 22 06 22 22 22 46 06 44 46 66 68
22 24 44 66 78 78 88 22 24 42 56 98 12 06 44 46 66 24 42

```

Figure 3.2.1  
Example of NMR Raw Data File

NMR data files contain 256x256 positive, even integers. Integers at the borders represent the noise in the image, while the integers in the center are the values used to process the image.

```

File Name       : ABX230.dat
Image Resolution : 256
Begin Row      : 1
End Row        : 256
Begin Col      : 1
End Col        : 256

```

```

82 66 24 44 66 78 78 88 22 24 42 56 98 12 06 44 46 66 68
56 98 12 06 44 46 66 68 12 12 44 56 66 22 06 22 22 22 46
66 24 44 66 78 78 88 22 24 42 56 98 12 66 68 12 12 44 56
66 68 12 12 44 56 66 22 06 22 22 22 46 06 44 46 66 68 12
12 14 22 26 34 46 56 66 78 68 98 46 56 20 10 30 70 90 20
46 56 66 78 68 98 46 56 20 10 30 70 90 20 82 66 24 44 78
234 238 122 100 120 150 134 122 128 142 154 132 444 446 444 498 500 100 12
122 554 234 334 346 456 678 568 566 556 346 788 566 344 324 334 232 122 13
166 334 546 556 788 998 888 778 668 444 444 446 556 778 888 778 676 556 55
178 568 566 556 346 788 566 344 324 334 232 122 134 456 788 444 442 122 55
178 668 444 444 446 556 778 888 778 676 556 556 222 122 778 668 444 444 44
188 778 676 556 788 998 888 778 668 444 444 446 556 778 888 778 676 556 55
234 334 346 456 678 568 566 556 346 788 566 344 324 334 232 122 134 456 78
156 788 998 888 778 668 444 444 446 556 778 888 778 676 556 998 888 778 66
146 556 778 556 788 998 888 778 668 444 444 446 228 388 346 734 654 542 44
158 676 556 788 998 888 778 668 444 444 446 556 778 888 778 676 556 556 55
144 446 556 778 888 778 676 556 556 222 122 778 668 444 444 444 446 22
134 654 778 676 556 788 998 888 778 668 444 444 446 556 778 888 346 788 56
334 232 122 234 334 346 456 678 568 566 556 346 788 566 344 324 334 232 12
788 166 334 546 556 788 998 888 778 668 444 444 446 556 778 556 778 888 77
78 78 88 22 24 42 56 98 12 66 68 12 12 44 56 78 12 22 22
06 44 46 66 68 12 12 22 56 66 78 68 98 46 56 20 10 30 70
22 12 68 12 12 44 56 66 22 06 22 22 22 46 06 44 46 66 68
22 24 44 66 78 78 88 22 24 42 56 98 12 06 44 46 66 24 42
E E E E E E E E E E E E E E E E E E
O O O O O O O O O O O O O O O O O O
C C C C C C C C C C C C C C C C C C

```

Figure 3.2.2  
Example of NMR Data File After Downloading

File Header contains information about each file such as file name, resolution, etc.

The data is downloaded one column at a time, and each column ends with EOC or end of column.

histogram of gray-level content<sup>23</sup>. The image enhancement is achieved by modifying the histogram of a given image in a specified manner. Figure 3.2.3 shows a typical histogram of an image. The curve represents the density function. The x-axis is the gray-level of pixels, which in our case ranges from 0 to 255. In the gray scale, 0 represents black, while 255 represent the white color pixels.

The gray levels in an image are random quantities in the range [0,255]. The density function of gray-level shows many characteristics of an image. Figures 3.2.4a and 3.2.4b show two examples of density functions. Figure 3.2.4a shows a predominantly light image since the majority of its pixels are light gray. Figure 3.2.4b, on the other hand, shows a density function of a dark image because the majority of its levels are concentrated in the dark region of the gray scale.

The purpose of histogram equalization is to produce an image whose gray levels have a uniform density. In terms of enhancement, this implies an increase in the dynamic range of the pixels, which produces a considerable change in the appearance of the image.

A histogram is a plot of the probability of the gray-levels as a function of the gray-level distribution in an image. NMR images consist of 256x256 matrices. A gray-level in the range [0,255] can then be used in processing the NMR data. The probability of any gray-level is the ratio of the number of times the particular gray-level appears in an image to the total number of pixels in that image. This relationship can be expressed as:

$$P_r(r_k) = \frac{n_k}{n} \quad \dots \dots \dots (3.2.1)$$

Where:  $0 \leq r_k \leq 255$

$$k = 0, 1, 2, \dots, L-1$$

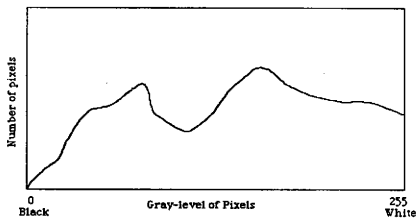
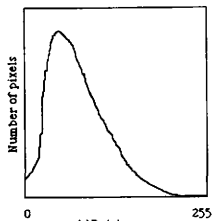
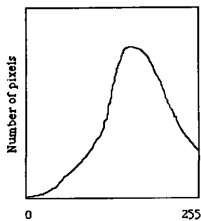


Figure 3.2.3  
Typical Histogram

x-axis : Gray-Level of Pixels.  
y-axis : Number of Pixels Having the Same Gray-Level.



(a) Dark Image  
Majority of Pixels Are Concentrated in the Dark Area



(b) Light Image  
Majority of Pixels Are Concentrated in the Light Area.

Figure 3.2.4  
Density Function

Histogram equalization requires performing calculations on huge amounts of data, therefore the process must be performed by a computer. A simplified example is given next to illustrate the procedure used in image enhancement.

### 3.2.4 Example

The following example presents and illustrates the histogram equalization. A 256x256, 255-level image has the gray-level distribution shown in Table 3.2.1

In this example, only 10 levels are allowed for illustration purposes. When processing NMR files, 255 levels are used due to the 8-bit color limitation on the Macintosh. The transformation function,  $S$  is obtained by:

$$S_j = \sum_{i=0}^j P_r(r_i) \quad \dots \dots \dots (3.2.2)$$

Where  $(i)$  is any gray-level in the image in the range  $[0,255]$ , and  $P_r(r_i)$  is the ratio of number of pixels with gray-level of  $(i)$  to the total number of pixels in the image. Ten transformation values will be produced when substituting the values in Table 3.2.1 into the transformation equation. The transformations values for the first two gray-levels can be presented as follows:

$$S_0 = \sum_{i=0}^0 P_r(r_0) = 0.14$$

$$S_1 = \sum_{i=0}^1 P_r(r_i) = 0.34$$



**TABLE 3.2.1**  
**Gray-level Distribution**

$r_k$	$n_k$	$P_r(r_k)$	S
0	09175	0.14	0.14
30	13107	0.20	0.34
60	15073	0.23	0.57
90	10485	0.16	0.73
120	05898	0.09	0.82
150	04587	0.07	0.89
180	03276	0.05	0.94
210	01966	0.03	0.97
240	01310	0.02	0.99
255	00655	0.01	1.00

**TABLE 3.2.2**  
**Results of the Transformation Function**

S	SX255	Gray-Level
0.14	035.7	30
0.34	086.7	90
0.57	145.3	150
0.73	186.1	180
0.82	209.1	210
0.89	226.9	240
0.94	239.7	240
0.97	247.3	240
0.99	252.4	255
1.00	255.0	255

Table 3.2.1 contains the transformation function for this example. Multiply the transformation function by 255 and each resulting value must be assigned to its closest valid level. The result is a set of new gray-levels different from the original set. Table 3.2.2 contains the results of this operation.

Gray-levels in Table 3.2.2 shows that only seven of 10 gray-levels are distinct. The first gray-level,  $S_0$  was transformed from 0 to 30. There are 9,175 transformed pixels with this new value. Also there are 13,107 pixels with value  $S_1 = 90$ , and 15,073 pixels with value  $S_2 = 150$ . There are also 10,485 of  $S_3 = 180$ .  $S_5, S_6$ , and  $S_7$  were mapped to  $S_5 = 240$ . There are now  $4,587 + 3,276 + 1,966 = 9,829$  pixels with this new value. Similarly, there are  $1,310 + 655 = 1,965$  pixels with value  $S_8 = 255$ .

Figure 3.2.5 is an illustration of the histogram equalization method. The original histogram data is shown in Figure 3.2.5a where the number of pixels is plotted as a function of the intensity distribution. The transformation function, which is the cumulative density function of Figure 3.2.5a, is shown in Figure 3.2.5b. Figure 3.2.5c shows the equalized histogram after applying the procedure.

### 3.2.5 Program

A program was designed to perform a histogram equalization and image enhancement on the data obtained from NMR experiments. Appendix A contains a list of the Algorithms used in this program.

Algorithm 1 performs a histogram plot on the 256x256 matrix (Gray-levels vs. the number of pixels having the same gray-level). The algorithm also determines the gray-level where the maximum number of pixels occur.

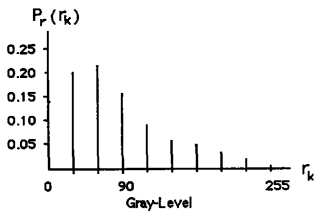


Figure 3.2.5a  
Original Histogram

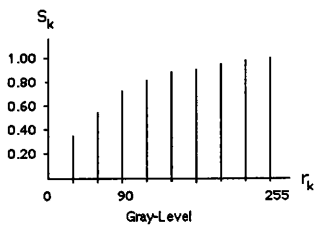


Figure 3.2.5b  
Transformation Function

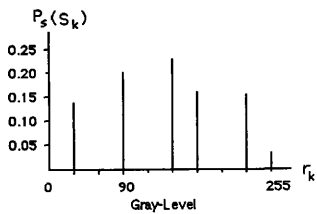


Figure 3.2.5c  
Equalized Histogram

Algorithm 2 determines the maximum noise value. This value is used as the start of the good data ( the data used to process the original image). The algorithm also calculates the total number of pixels in the noise area.

Algorithm 3 determines the total number of pixels that can be used in developing the new enhanced image. The Algorithm also assigns the range of gray-levels allowed in the new image.

The last algorithm assigns gray-levels to each pixel in the image. The assignment process can be accomplished by expanding the gray-levels between the start of the good data and the maximum data level in order to remove the noise level. The 256x256 matrix can be saved as a binary file once the noise level has been set to a constant value.

The procedure is illustrated in Figure 3.2.6. The figure shows the different gray-levels in a histogram. As shown in the figure, line (c) is where the good data starts. Line (d) marks the gray-level where the maximum number of pixels occurred. Area (A) is the noise area which is usually removed to reduced the noise level and enhance the image. The area marked (B) is the region used in the new image by expanding its gray-level. Appendix B contain four Charts to illustrate how the four algorithms work.

Figure 3.2.7 is an example of the images produced by this process. The image is a longitudinal cross section in the core. The dark area in the image represents the oil saturation in the core. The darker the color, the higher the saturation of oil. As shown in the figure, the core did not occupy the whole area of the image. The region surrounding the cross section of the core is not useful, and it represents the noise that was discussed earlier. This noise was reduced sufficiently so that the image can be studied easily.

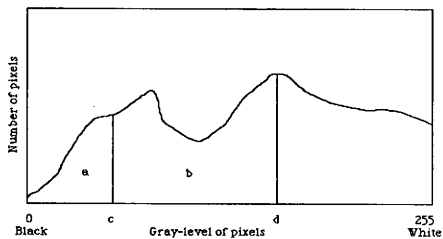
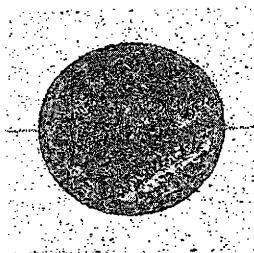


Figure 3.2.6  
Typical Equalization Mechanism

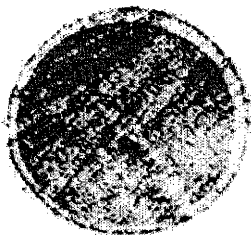
x-axis: Gray-level of pixels.

y-axis: Number of pixels having that gray-level.

- a : Noise area ( To be set constant).
- b : Good data ( To be used in the image).
- c : Gray-level where good data starts.
- d : Gray-level at maximum number of pixels.



(a) NMR Image with Noise



(b) Image Produced from the Method Discussed

Figure 3.2.7  
Example of an Image Produced by the Method Discussed.

### **3.3 Image Processing Functions**

This section, Image Processing Functions, starts with a discussion of the two methods used in image processing. A summary of some of the functions used in this research with some example also included.

#### **3.3.1 Processing Methods**

Image processing depends on the interchange of information between pixels. This is easily achieved with the local connectivity of the array of pixels. The basic image transformation can be broadly divided into two categories. The first depends on each pixel's relationship with its immediate neighbors, a property which utilizes local propagation. The second uses the notion of global propagation where information can be passed right across the array of pixels<sup>24</sup>.

The main objective of enhancement techniques is to process a given image so that the result is more suitable for interpretation than the original image. Two major categories of image processing are discussed in this section: frequency-domain methods and spatial-domain methods. Processing techniques in the first category are based on modifying the Fourier transform of an image. The spatial domain refers to the image plane itself and processing techniques are based on direct manipulation of the pixels in the image.

#### **3.3.2 Spatial-Domain Methods**

Spatial-domain refers to the plane of pixels that composes the image. The spatial-domain methods are procedures that operate directly on the pixels of an image by manipulating them. The result is usually a new image which has some relationship with the original image. The



procedure operating on an image may contain one or more functions. An image processing function in spatial-domain may be expressed as:

$$g(x,y) = O[f(x,y)] \quad \dots \dots \dots (3.3.1)$$

where  $f(x,y)$  is the input image,  $g(x,y)$  is the processed image, and  $O$  is the operation that is performed on the original image,  $f$ . Usually the operation is performed on each pixel separately. Neighboring pixels are also taken into consideration. The neighboring pixels about  $(x,y)$  are usually considered to be a square or rectangular sub-image area centered at  $(x,y)$ . Figure 3.3.1 shows a 3x3 sub-image area that can be processed to produce the new pixel  $(x,y)$ .

The simplest operation that can be performed on an image is when the sub-image is 1x1 area. In this case,  $g$  depends only on the value of  $f$  at the point  $(x,y)$ . An example of this operation may be the transformation of a multi-gray-level image into a two-gray-level image. Figure 3.3.2a shows the distribution of brightness as a function of gray-level. This distribution can be transformed into a higher contrast image by darkening the levels below a value  $m$ , and brightening the levels above it in the original image. The result of this operation is shown in Figure 3.3.2b. The levels of pixels below  $m$  are compressed by the transformation function toward the dark end of the spectrum, while the opposite effect takes place for the values above  $m$ . Figure 3.3.2c is an NMR image with multi-gray-level [0-255]. The result of the transformation using  $m=128$  is shown in Figure 3.3.2d.

Larger sub-images allow a variety of processing functions. In this case, the values of  $f$  in the neighborhood of  $(x,y)$  determines the values of  $g$  at that pixel. The function is not performed on the pixel  $(x,y)$ , but it is performed on the sub-image surrounding the pixel  $(x,y)$ <sup>25</sup>. For example, assume we have an image of constant intensity and we need to detect

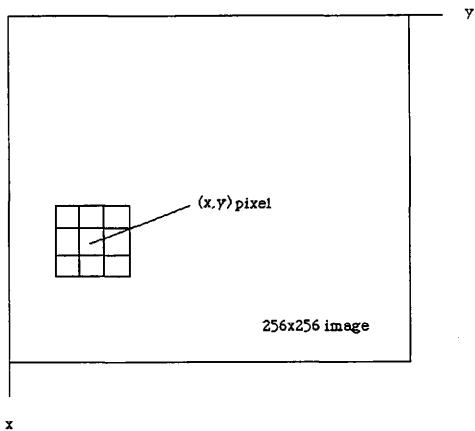


Figure 3.3.1  
A 3x3 Neighborhood About a Pixel  $(x,y)$   
in a 256x256 image.

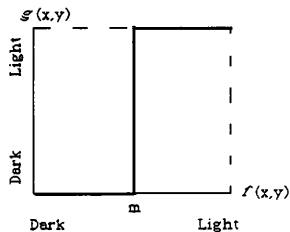
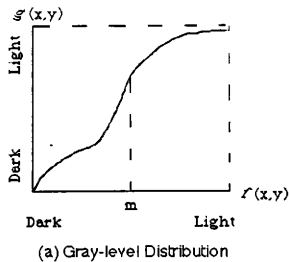


Figure 3.3.2  
 Gray-Level Transformation Function  
 for a 1x1 Sub-Image.



(c) NMR Image  
Gray-Level in the Range [0-255]



(d) NMR Transformed Image  
Gray-Level in the Range [128-256]

Figure 3.3.2  
Continued

any points in the image with different intensities. This operation can be performed by using the sub-image shown in Figure 3.3.3. The procedure requires moving the sub-image of Figure 3.3.3 around in the image. Every pixel in the image is multiplied with the corresponding pixel in the sub-image at each location in the image. The result of the nine multiplications is then summed. The sum will be zero if all the pixels within the sub-image area are equal. Figure 3.3.4 outlines this procedure.

The sub-image in Figure 3.3.3 represents the *function* that operates on each pixel of the original image. If we let  $S_1, S_2, \dots, S_9$  represent the function coefficients and consider the eight surrounding pixels of  $(x,y)$ , we may generalize a mathematical function  $O$  that will perform this operation. Adding the elements of Figure 3.3.5, the function can be written as:

$$\begin{aligned} O[f(x,y)] = & S_1f(x-1,y-1) + S_2f(x-1,y) + S_3f(x-1,y+1) \\ & + S_4f(x,y-1) + S_5f(x,y) + S_6f(x,y+1) \\ & + S_7f(x+1,y-1) + S_8f(x+1,y) + S_9f(x+1,y+1) \dots \quad (3.3.2) \end{aligned}$$

### 3.3.3 Frequency-Domain Methods

Frequency-Domain image processing is based on the convolution theorem which emphasizes the fact that the resulting image depends only on the value of the original image at a given point in the image and not on the position of the point <sup>26</sup>. If  $g(x,y)$  is an image formed by applying an operator  $h(x,y)$  on the original image  $f(x,y)$ , that is,

$$g(x,y) = h(x,y) * f(x,y) \dots \dots \dots (3.3.3)$$

-1	-1	-1
-1	8	-1
-1	-1	-1

Figure 3.3.3  
A 3x3 Sub-Image.

23 -1 -23	23 -1 -23	23 -1 -23	23	23
23 -1 -23	23 8 184	23 -1 -23	23	23
23 -1 -23	23 -1 -23	23 -1 -23	23	23
23	23	23	23	23
23	23	23	23	23

Figure 3.3.4  
Procedure for Detecting Variations in Gray-level in an Image.

- 1) Move the center of the  $3 \times 3$  subimage to the first pixel.
- 2) Multiply each pixel in the image with the correspondent pixel in the subimage. (e.i.,  $23 \times 1 = 23$ , and  $23 \times 8 = 184$ ).
- 3) Add the resulting value for the nine pixels.
- 4) If the summation = 0, the nine pixels in the image have the same value.
- 5) Move the center of the  $3 \times 3$  subimage to the second pixel in the original image, and repeat steps 2-4.

$S_1$ $(x-1, y-1)$	$S_2$ $(x-1, y)$	$S_3$ $(x-1, y+1)$
$S_4$ $(x, y-1)$	$S_5$ $(x, y)$	$S_6$ $(x, y+1)$
$S_7$ $(x+1, y-1)$	$S_8$ $(x+1, y)$	$S_9$ $(x+1, y+1)$

Figure 3.3.5  
Image Pixel Locations and  
Coefficients of Sub-Image.



The frequency-domain relation is:

$$G(x,y) = H(x,y) * F(x,y) \quad . . . . . (3.3.4)$$

Where  $G$ ,  $H$ , and  $F$  are the Fourier transforms of  $g$ ,  $h$ , and  $f$ .  $H(x,y)$  is called the transfer function of the process. In a typical image enhancement problem,  $f(x,y)$  is given and  $F(x,y)$  can be calculated.  $H(x,y)$  has to be selected to produce the desirable  $g(x,y)$ . Both  $H(x,y)$  and  $h(x,y)$  have to be of the same size. An equivalent spatial results will be produced only if  $h(x,y)$  is a 256x256 image if  $H(x,y)$  is a 256x256 image.

There is no general theory of image enhancement. The viewer is the only judge of how well a particular method works when an image is processed for visual interpretations. Visual evaluation of image quality is a highly subjective process, thus the same method may be judged differently by different users.

### 3.3.4 Local Enhancement

The two methods discussed earlier are global because pixels are modified by a transformation function based on the gray-level distribution over an entire image. Global methods are very appropriate for overall enhancement. It is important to enhance detail over a small area of the image as well. Local enhancement is based on the transformation of the pixel in a small area with respect to its immediate neighboring pixels<sup>27</sup>.

The procedure for local enhancement is to define an  $n \times m$  neighborhood and move the center of this area from pixel to pixel. At each location, the enhancement is performed over the specified area. The center of the  $n \times m$  region is then moved to an adjacent pixel location and the enhancement procedure is repeated.

An illustration of local image enhancement with the neighborhood moved from pixel to pixel is shown in Figure 3.3.6. Part (a) of the image shows an image that has been blurred to reduce the noise level. Part (b) shows the result of a 7x7 local equalization. More detail features of the image is shown.

### 3.3.5 Image Smoothing

Smoothing operations are used for reducing the noise effects that may be present in an image because of poor resolution. Image smoothing can be accomplished by a variety of techniques such as neighborhood averaging, median filtering, and low-pass filtering.

#### 3.3.5.1 Neighborhood Averaging

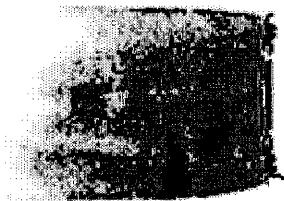
Neighborhood averaging is a spatial-domain technique for image smoothing. The purpose of this technique is to generate a smoothed image  $g(x,y)$  given an  $n \times n$  image  $[f(x,y)]$ . The gray-level at each pixel is  $(x,y)$ , and is obtained by averaging the gray-level values of the original image contained in a predefined area. The transformation can be presented with the following function:

$$g(x,y) = \frac{1}{M} \sum_{(n,m)} f(n,m) \quad \dots \dots \dots (3.3.5)$$

where  $x$  and  $y$  are the pixel locations in the new image,  $(n,m)$  is the predefined neighborhood in the original image, and  $M$  is the total number of points in the neighborhood <sup>28</sup>. The averaging, for a 3x3 neighborhood, will be in the following form:



(a) Original NMR Image  
Cross Section in a Core Sample.



(b) A 7x7 Local Equalization of the NMR Image

Figure 3.3.6  
Local Image Enhancement Example

$$g(x,y) = \frac{1}{9} \sum_{\substack{m=3 \\ n=3 \\ m=1}}^{m=3} f(n,m) \quad \dots \dots \dots (3.3.6)$$

Figure 3.3.7 is an illustration of neighborhood averaging function. Part (a) is the original image of a cross section of a core flooded with both oil and D<sub>2</sub>O .

### 3.3.5.2 Median Filtering

Median filtering is an improved approach of the neighborhood averaging method. The technique is based on replacing the gray-level of each pixel by the median of the gray-levels in a neighborhood of that pixel, instead of by the average<sup>29</sup>. Median  $m$  of a set of values is the value where half the values in the set are less than  $m$  and the other half are greater than  $m$ . The procedure can be simplified by the following function:

$$g(x,y) = \frac{f_{M+2}(x,y)}{2} \quad \dots \dots \dots (3.3.7)$$

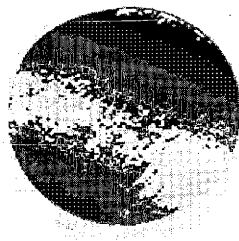
where  $M$  is the total number of pixels in the predefined area, and  $\frac{f_{M+2}}{2}$  is the  $(\frac{M+2}{2})^{\text{th}}$  gray-level when the gray-levels of the  $M$  pixel are sorted. Figure 3.3.8 shows the results of this technique.

### 3.3.5.3 Low-Pass Filtering

Low-pass filtering is the method used to enhance the gray-levels of a low-frequency content of an image. High-frequency components are filtered out and information in the low-frequency range is passed<sup>30</sup>. The point of transition between the high and low frequencies which is called



(a) Original NMR Image  
Cross Section of a Core Sample.

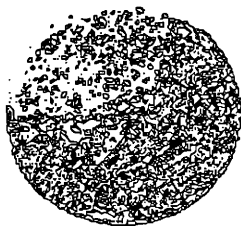


(b) Neighborhood Averaging Method

Figure 3.3.7  
Neighborhood Averaging Function



(a) Original NMR Image  
Cross Section of a Core Sample.



(b) Median Filtering Results

Figure 3.3.8  
Example of a Median Filtering Operation.

the cut-off-frequency, can be chosen so the noise level is reduced. Figure 3.3.9 is an illustration of low-pass filtering.

### **3.3.6 Statistical Functions**

Public domain programs are provided with routines to perform a variety of statistical functions on a selected region or the total area of the image. Those functions relate the pixel intensity to the number of pixels in the selected area. Statistical functions, in terms of fluid flow, provide both quantitative and qualitative information of the fluid distribution as a function of location.

#### **3.3.6.1 *Density Profile***

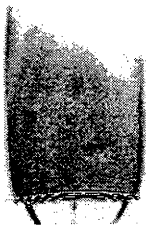
A density profile produces graphical plots of the gray-level along a line which is generated between two points. The saturation of the fluid in the core can be determined at any position in the image by simply drawing a line at that location. This function can be used to get saturation profiles and compare the saturations along the core at the time the image was taken<sup>31</sup>. Figure 3.3.10 explains density profile plots.

#### **3.3.6.2 *Average Density Profile***

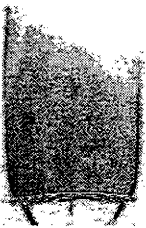
An average density profile provides density profiles for a rectangular area. Initially, the function averages the gray-levels in one dimension, and then plots the averaged intensities as a function of the other dimension<sup>31</sup>. An average fluid saturation of a selected area or the total area of the image can be useful in determining the saturation in the direction of the image as shown in Figure 3.3.11.

#### **3.3.6.3 *Histogram Profile***

Histogram profiles display, for each of the 256 possible gray-levels, the number of pixels within the selection area that have the gray-



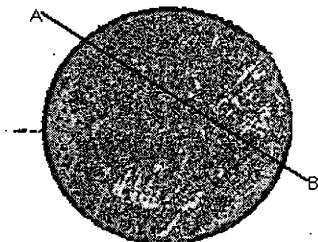
(a) Original NMR Image



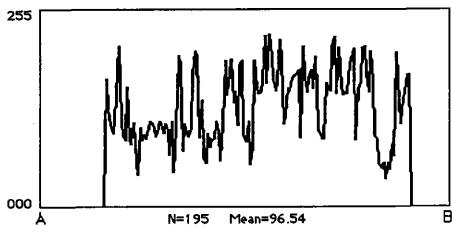
(b) Low-Pass Filtering

Figure 3.3.9  
Example of Low-Pass Filtering





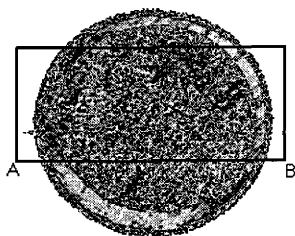
(a) 0-256 Gray-level NMR Image



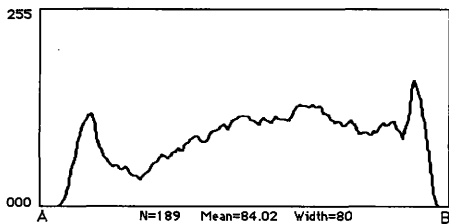
(b) Density Profile Plot

N = Number of Pixels Between A&B  
Mean = Mean of Gray-level Distribution

Figure 3.3.10  
Density Profile



(a) 0-256 Gray-Level NMR Image



(b) Average Density in Rectangle.

N = Number of Pixels Between A&B  
Mean = Mean of Gray-Level Distribution.

Figure 3.3.11  
Average Density Profile

level<sup>32</sup>. Histogram plots show the saturation ranges of the different fluids. See Figure 3.3.12 for more explanation.

#### 3.3.6.4 *Contour Maps*

Contour mapping is an easy way to show the distribution of ranges of different saturations in the image. Contour maps connect the pixels of the same saturations. The interval between the different contour lines may vary as much as the gray-level; in our case, 256 resolution images may vary from 0 to 255<sup>33</sup>. Some examples of contour maps are shown in Figure 3.3.13.

#### 3.3.6.5 *Saturation Front*

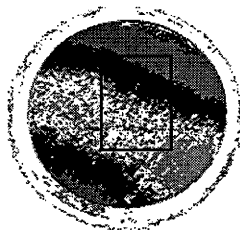
This function displays the fluid saturation front or the two-phase contact line. The operation of the function is based on the fact that the contact line between two phases usually encounters a noticeable change in pixel intensity. Appendix C contains a listing of the Algorithm of the fluid front function. An example of saturation front image produced by this function is shown in Figure 3.3.14.

#### 3.3.6.6 *Mean*

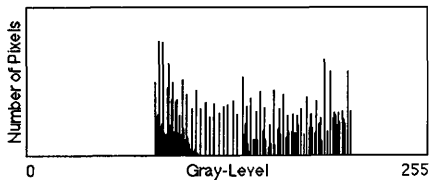
The Mean produces an arithmetic average of the intensity in a specified region. The area can be of any dimension, shape, or size as long as it has one or more pixels in it. Figure 3.3.15 is an illustration of this function.

#### 3.3.6.7 *3D Plot*

The 3D function provides a plot of the image intensity<sup>34</sup>. It consists of a 2D image with the pixel intensity in the third dimension as shown in Figure 3.3.16 and Figure 3.3.17.

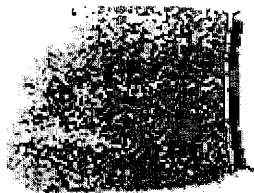


(a) NMR Image



(b) Histogram Plot

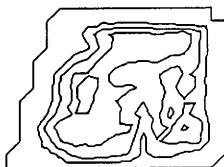
Figure 3.3.12  
An Example of Histogram Plot.



(a) NMR Image



(b) Contour Line = 25



(c) Contour Line = 50

Figure 3.3.13  
Contour Maps

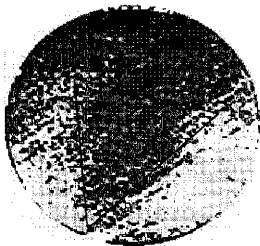


(a) Saturation Image



(b) Saturation Front

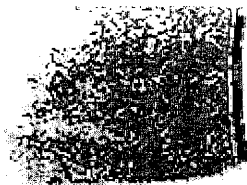
Figure 3.3.14  
Saturation Front Example.



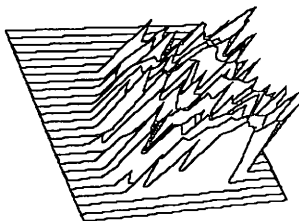
For the region specified

AREA	4891
MEAN	82.28
ST. DEV.	65.340
INTEGRATED DENSITY	402453

Figure 3.3.15  
Arithmetic Average.



(a) NMR Image



(b) 3D Plot

Figure 3.3.16  
An Example of 3D Plot.



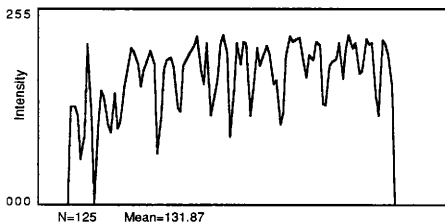


Figure 3.3.17  
Average Intensity of 3D Plot in Fig. 3.3.16

### **3.4 Summary**

A summary of image processing methods is discussed in this section. Image processing functions are explained in terms of fluid flow in porous media.

#### **3.4.1 Experimental Results**

Nuclear Magnetic Resonance (NMR) imaging techniques are used to measure changing fluid saturations and relative permeabilities in porous materials. The recorded signals are a measure of the volumes of the fluids residing in the pore spaces

Most NMR systems use expensive interactive work stations for data manipulation and image analysis. The technique of interpreting NMR data permits a color Macintosh to be used in place of more expensive, graphics work-stations. The technique was developed and tested in the Petroleum Engineering Department, and is being used in research projects at the present time. The process produces images with sufficiently good resolution to distinguish features within the image.

The Macintosh system provides a fairly inexpensive image processing capability that accomplishes 80% of the functionality of a system that is 5 to 6 times the cost. Relying on public domain software and in-house developed programs, researchers have been able to carry out research that might normally have been financially out of reach.

#### **3.4.2 Image Saturation**

The signal obtained from the NMR is a measure of the volume of oil contained in the measured pore volume. The intensity of the signal is

proportional to the detected oil volume. Thus, the signal is a function of the oil saturation in the imaged section.

Three different NMR image sections were taken: Cross sections, longitudinal sections, and horizontal sections. All NMR images that were produced during this research had a 256 resolution; that means the gray-level of the image pixels ranged from 0 - 255. A gray-level of 0 represents zero oil saturation or 100% D<sub>2</sub>O saturation. A 100% oil saturation is represented by gray-level of 255. This gray-level can, however, be scaled to 0-100 oil saturation.

The oil saturation distribution in the image can easily be studied by using the scales gray-level of the image. Density plots as well as contour plots are very helpful in understanding the distribution of the oil saturation in the core. Figure 3.4.1 is a longitudinal cross sectional image in a core sample flooded with both oil and D<sub>2</sub>O. Oil saturation profiles across the image were taken at different positions along the flow stream. Figure 3.4.2 shows the saturation profiles in the image. The figure shows that the oil saturation decreases from right to left.

Contour maps provide better understanding of the distribution of oil in the selected section. The contour lines connect pixels of equal oil saturations. Thus, regions of equal saturations can be visualized. Figure 3.4.3 is a contour map of the image shown in Figure 3.4.1.

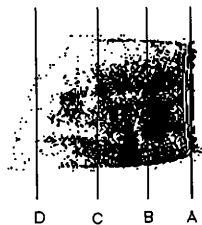


Figure 3.4.1  
NMR Longitudnal Image.  
Saturation Decreases From Right to Left.

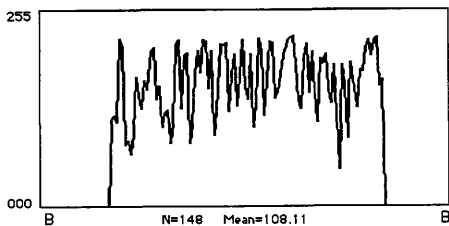
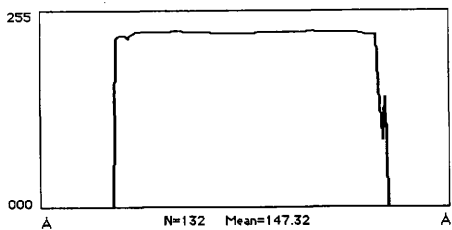


Figure 3.4.2  
Saturation Plot

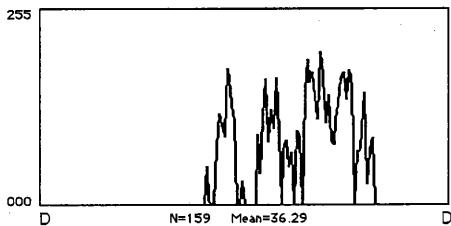
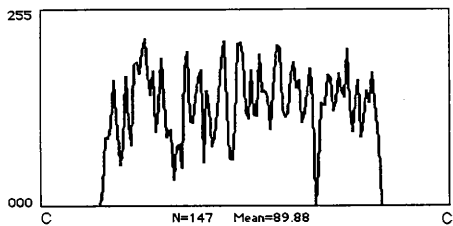


Figure 3.4.2  
Continued

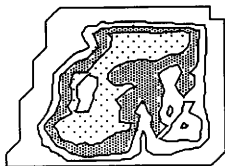


Figure 3.4.3  
Contour Map for the NMR Image in Figure 3.4.1  
Contour Interval of 50.

## **CHAPTER IV**

### **APPLICATIONS OF NMR IN FLOW BEHAVIOR**

This chapter contains some of the applications of the NMR imaging techniques in the study of flow behavior of fluids and their properties. Section 4.1 is an introduction to the concepts of fluid saturation, relative permeability, and imbibition flooding. It provides a literature review of the different methods used to study those properties. Section 4.2 describes fluid saturation in terms of the NMR signals obtained during the flooding experiments. Equations developed to measure fluid saturation were used in measuring relative permeability in section 4.3. The behavior of fluid in water-wet rock is introduced in section 4.4.

#### **4.1 Introduction**

This section is a literature review of flow behavior in porous media. A discussion of the equipment setup and the laboratory experiment is included as well.

##### **4.1.1 Reservoir Properties**

Development of petroleum reservoirs was more of an art than science in the early stages of the industry. More efficient utilization of these natural resources is needed. The technological advancements in this field has been tremendous in a relatively short period of time. The problem presented by the existence of oil together with other fluids in the pores of rocks having extremely complex network of flow paths. This problem has provided a challenge for engineers and scientists to devise methods for optimizing the production and maximizing ultimate recovery. In the early stages of oil production, the pressure had to be regulated to conserve the only driving energy, but at the same time a reasonable production has to take place for a profitable operation.



Means of secondary recovery were developed to recover part of the large amounts of petroleum that is usually left in place after the primary operations. Various methods of secondary recovery have been developed throughout the history of oil industry. Some of these methods include water flooding, gas drive, underground combustion, miscible flooding, and others <sup>35</sup>. With all these available techniques, a reservoir engineer needs to know the physical and chemical properties of both the reservoir rocks and the reservoir fluids. These properties are needed so the reservoir engineer will be able to determine under given conditions how permeable the reservoir rock is to a particular fluid at any time in the history of the reservoir. When more than one fluid is flowing simultaneously.

Several rock and fluid properties need to be studied before one is able to determine how permeable a rock is to a particular fluid. Rock properties including porosity, compressibility, and the presence or absence of fracture are important for the determination of the type of reservoir rock. Fluid properties such as initial saturations of fluids in the rock, viscosity and density of each fluid, and other properties relating the different fluids together are also needed for any reservoir study. Relating fluid properties to rock properties is rather important in determining the flow behavior of the reservoir fluids and the relative permeability to each fluid.

#### **4.1.2 Oil Saturation**

Oil shale is a rock of sedimentary origin, and contains both inorganic and organic materials. There are several types of oil shale. Torbanites are the richest type because they yield the most oil and have the highest organic content <sup>36</sup>.

A reservoir initially is filled with oil and water when no initial gas cap is present. Usually, the water content is determined from use of logs, capillary pressure, and core information. Porosity can be determined from cores, logs, and other available techniques. Later during productive

life, gas will be present when oil is below its bubble point. The determination of saturation values of oil and gas can be difficult.

Naturally oil, water and gas are segregated so that the fluids are located according to their densities. Density or gravitational forces place gas at the top, oil in the middle, and water at the bottom. Gas and oil, however, can be trapped in different locations in the reservoir. The time of migration and accumulation of gas and oil within the water-filled aquifer controls the location of the small oil and gas reservoirs within traps in the area filled with water. Gas can displace an oil accumulation, and an oil accumulation may leak from a faulty trap. The residual oil saturation is the oil saturation remaining in water or gas-swept zones. Methods for measuring residual oil saturation include:

- 1) Core analysis.
- 2) Coring techniques.
- 3) Reservoir engineering studies.
- 4) Logging, and
- 5) Pressure transient analysis.

Residual oil saturation is very critical in the economic evaluation of reservoirs. Large areal variations in oil saturations remaining in reservoirs should be studied. Water saturation is usually measured using logging techniques. The values of water saturation is usually used to determine the oil saturation in a reservoir.

#### **4.1.3 Water Saturation**

Water saturation is usually obtained from resistivity logs, capillary pressure information, and routine core analysis. Porous formations contain water when buried. Most formations were deposited in a marine environment and all rocks are saturated with water mixed with air.

Oil and gas from shale and other possible sources migrated with water as mobile fluids were displaced to new locations. Oil and water

migrates from shales as a result of the reduction of porosity associated with compression of the rocks. Gravity and other forces caused the oil to become small droplets, which increased in size to form oil accumulations.

Oil has displaced the original water from the pores of the rock so that there is equilibrium between gravity and capillary forces in most reservoirs. The water saturation is highest near the oil-water contact and gradually decreases with height as oil saturation increases.

Gas can displace both oil and water, while oil can displace only water from the formation. The oil, gas and water contents of cores are routinely determined during laboratory analysis. Resistivity logs are the most frequently used method for determining in-place water at any time. The water saturation from resistivity logs is based on the fact that the resistivity of formation is proportional to the resistivity of water in the formation.

#### **4.1.4 Permeability**

Reservoir engineers are always challenged to provide means to optimize production and maximize ultimate recovery. Pressure, which is the driving force, drops as a result of the production of oil. A drop in reservoir pressure has to be regulated to conserve the driving energy. A reasonable amount of oil, however, has to be produced to maintain economical operations in the field. Secondary recovery methods are needed, in later stages of production history, to recover as much as possible of the oil that is still left in the reservoir after the primary operations. Various methods of secondary recovery are now in use, such as gas drive, water flooding, underground combustion, miscible displacement, and others. Under any of those conditions, the reservoir engineer needs to know how permeable the reservoir rock is to the fluids flowing through its rocks.

Any laboratory method of determining relative permeability must meet, among others, the following minimum requirements <sup>37</sup>:

- 1) The core saturation between the pressure taps must be uniform.
- 2) There must be uniform pressure difference between the phases in the region between the pressure taps.

In practice it may be shown that appreciable departure from either or both of these conditions may be permitted without introducing sensible error, but the magnitude of such error remains to be established.

The best values for permeability are usually obtained from flow and buildup testing. Permeability may be directly measured in the laboratory using representative cores that have been properly handled so that in-situ conditions are preserved. Values obtained from laboratory tests must be properly averaged.

The presence of capillary fluid reduces the air permeability as measured in the laboratory. Relative permeability concept must be used when two or more fluids are flowing at the same time.

#### **4.1.5 Imbibition Flooding**

Imbibition has been recognized as an important factor in recovering oil from water-wet, fractured-matrix reservoirs subjected to water flooding or water drive. The process of water-imbibition displacement is slow, but it is often regarded as an important mechanism in the recovery of oil. A number of methods have been published which might be used to predict the imbibition oil recovery behavior for reservoirs.

Brownscombe and Dyes <sup>38</sup> performed laboratory studies on imbibition flooding in 1952. Their studies showed that the imbibition flooding could increase recovery from highly a fractured reservoir. it was

concluded that the matrix must be water-wet so that natural water imbibition will occur.

Graham and Richardson <sup>39</sup> used a synthetic model to scale a single element of a fractured matrix reservoir. Blair, <sup>40</sup> on the other hand, used numerical techniques to solve the differential equations describing imbibition in linear and radial systems. This latter method requires auxiliary experimental data in the form of capillary pressure and relative permeability functions.

A third method for predicting imbibition oil recovery for large reservoir matrix blocks was presented by Mattax and Kyte <sup>41</sup>. Experimental work verifying imbibition recovery theory as related to the matrix block size, viscosity and permeability was also presented. This method uses scaled imbibition tests on small reservoir core samples to predict field performance. The imbibition tests are easier to perform than the capillary pressure and relative permeability tests required to apply the numerical method.

Tracers have been used to locate flow paths in a pilot flood. The ideal tracer would follow the fluid of interest exactly, traveling at the same velocity as the fluid front. But the ideal is impractical to attain because adsorption-desorption effects cause the tracer to lag behind the front. These effects cause the tracer front to spread more than the fluid front <sup>42</sup>.

#### **4.1.6 Equipment Layout**

A 2 5/8" diameter and 5 7/8" long dolomite core sample was used in this study. D<sub>2</sub>O was used instead of water to obtain a response for oil only.

The dry sample and two lucite ends were wrapped with epoxy. A fractured matrix face was simulated by indenting a 1/8" space into the

lucite ends, creating an imbibition face. Figure 4.1.1 is a sketch of the core sample in the core holder ready to be placed in the magnet. The NMR signal obtained from the 1/8" oil reservoir was used to calibrate the NMR signal. The NMR signal was scaled to obtain the oil saturation in the image since the signal obtained from this oil reservoir represents 100% oil.

A D<sub>2</sub>O flood was performed until a maximum D<sub>2</sub>O saturation was achieved. An oil flood was then performed to obtain maximum oil saturation. Longitudinal and cross sectional NMR imaging were performed on the sample as the saturation of oil increased in the core sample.

Figure 4.1.2 illustrates the layout for the fluid flow system. As shown in the figure, two fluids (oil and D<sub>2</sub>O ) are entering the core. The flooding experiment was conducted by displacing one fluid by the other. The output flow was collected in a beaker and its volume was measured.

The layout of NMR spectrometer and the equipment needed to run the flow experiment is shown in Figure 4.1.3. The core sample is placed inside of the magnet after being inserted inside the rf coil. Compressed nitrogen was used to control the temperature of the magnet. Two constant displacement pumps with variable rates were employed to provide flow of the two liquid phases, oil and water. Oil was pumped directly into the 1/8" thick reservoir at the face of core. The effluent from the core was collected in a separate vessel. Electronic pressure transducers were connected to the two pressure taps which measured the upstream and downstream pressure across the core sample. The signals obtained from the sample by the coil are analyzed by the computer using Fourier transform.

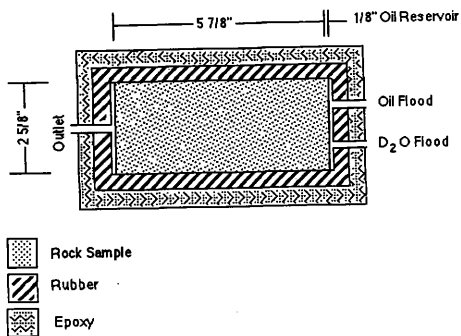


Figure 4.1.1  
Core Holder.

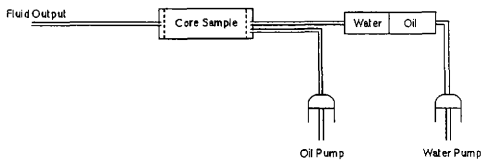


Figure 4.1.2  
Layout of Flow System.



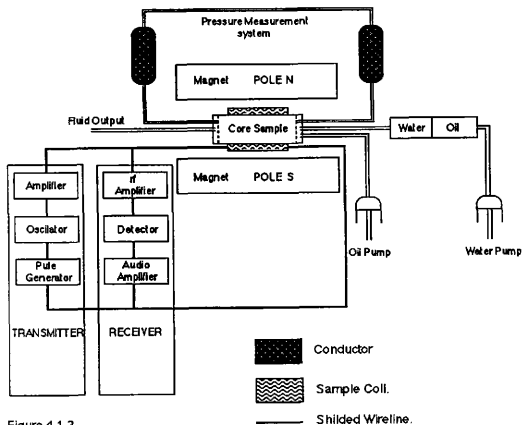


Figure 4.1.3  
Layout of NMR Flow Experiment

## 4.2 Fluid Saturation

This section discusses the various methods of measuring fluid saturation in porous media. A discussion of the NMR techniques and its advantages is also included. An equation was also developed to calculate fluid saturation from the NMR image.

### 4.2.1 Methods of Measurements

There is a need for methods of saturation determination which will determine the saturation profile in a core as well as the overall average saturation given by the gravimetric or material balance methods. The problem with fluid saturation determination in multiphase flow studies has been given extensive attention. Essential requirements for an acceptable method are:

- 1) The measurements are made external to the porous rock sample .
- 2) Saturation values must be independent of the fluid distribution in the core.
- 3) Several independent measurements along the core are usually required.
- 4) The properties of the fluids in the core sample should not be influenced by the experiment.

Several methods meet those requirements. Resistivity, X-ray absorption, gamma ray absorption, radioactive tracers, and neutron diffraction are some of the methods used to measure the saturation values..

Those methods have been discussed in the petroleum literature in detail. The problem with those methods is that they can not be used to study the fluid distribution in the core sample <sup>43</sup>. Flow patterns of the

fluids in the rock as a function of both location and time can not be studied using those methods.

The use of magnetic tracer in one of the fluids is required since fluids used in multiphase flow studies involving petroleum reservoir samples possess low magnetic susceptibilities. The relatively high magnetic susceptibility of salts and their high water solubility makes water the logical choice as a tracer material. The water saturation is determined and the value obtained is used to calculate the oil saturation in the core sample.

Interpretations of the SP log in terms of formation water resistivity is based on the fact that the observed SP is equal to the electrochemical potential developed across a shale between the mud filtrate and the formation water <sup>44</sup>. The SP log values are not very accurate because of the reduction of magnitude of the SP by formation geometry and resistivity effects.

Resistivity and conductivity logs are both based on the water in the formation, and the values obtained from them are influenced by any external fluids such as drilling mud<sup>44</sup>. Thus, when measuring the saturation of water using log techniques, the logging engineer has to decide whether the water encountered by the logging device is the original reservoir water or a mixture of the original reservoir water and the water invaded the information as a result of drilling operations.

Mud logging is based on identifying the fluid content of formations during drilling. This method gives fast results, however it is influenced by a variety of factors such as:

- 1) Magnitude of hydrocarbon.
- 2) Rate of penetration.
- 3) Drilling mud properties.
- 4) Formation pore pressure.
- 5) Reservoir rock properties.

A possible disadvantage of the radioactivity method is that a disproportionate amount of the activity comes from the portion of the core nearest the counter.

It has been recognized that the nature and sequence of changes in fluid saturation in porous media play an important part in fluid flow behavior. These changes, which have been described as saturation history, should be considered when planning studies of such phenomena. It is desirable to duplicate as nearly as possible the reservoir saturation conditions before initiating fluid flow studies. The core saturation should be brought to the restored state condition in relative permeability experiments designed to simulate conditions of oil production. The correct saturation history permits the distribution of gas, oil, and water in pores of the proper sizes. The distribution of the fluids within the pores appears to affect the relative permeability results, the pressure difference between the phases, the mobility of the fluids, the time necessary to reach equilibrium, and the residual oil.

#### **4.2.2 Advantages of NMR Techniques**

NMR can nondestructively image a variety of chemical and physical properties of porous rocks and multiphase flow of fluid within a core. The technique can be used to distinguish between water and oil since the signals obtained from the NMR are a measure of the volume of the oil, and are not affected by the water. The method can also be used to measure residual oil when the core is flushed totally with water because the signals recorded is influenced only by the oil. NMR techniques can actually be used to visualize the flow patterns of the different fluids flowing in the core. The distribution of fluids does not affect the saturation value obtained

One advantage of the NMR techniques that can not be accomplished by other methods is that flow performance and saturation can be determined microscopically. The thickness of the NMR image can

be as small as 1 millimeter which will enable us to take a series of images in the core to actually visualize the flow patterns.

#### **4.2.3 NMR Techniques**

Nuclear Magnetic Resonance techniques have been used successfully to study the flow behavior of fluids in porous media. A relationship between both proton relaxation times and signal intensity for hydrocarbon and  $D_2O$  confined to rock pore spaces and the fluid saturation in the rock has been studied.

This methods relates the signal intensity [which are produced by processing the relaxation times] of each pixel in an image to the physical properties of the fluids in the pores of the rock. Application of this technique permits a histogram plot of the saturation front to be determined from the intensity profile.

The determination of oil saturation in a reservoir is one of the primary objectives of a reservoir engineer when studying a reservoir. Several methods have been developed to determine the different fluid saturations in a reservoir based on the saturation in a rock sample. The methods used at the present time are either from lab experiments or well logging data. Fluid saturation distribution has been a major research subject under study since the development of the NMR.

The signal recorded for each pixel using NMR methods is obtained directly from fluids contained in the pores of a rock. A proper understanding of the relationship between the physical properties of the rock and the observed response of the signal intensity is essential in determining the correct two phase fluid saturations. Understanding of the gradient of signal intensity within the image is also necessary to be able to distinguish between two or more different fluids in the rock.

Accuracy and confidence of the NMR interpretations can be further enhanced by reprocessing the signal intensity data. The noise level in

the image must be reduced, and the intensity of the features in the image must be enhanced to a degree where the different flow paths can be observed by reprocessing of the data.

#### 4.2.4 NMR Images

Signals produced by the NMR represents the volume of hydrogen ions contained in a pore space. These signals are processed using a 2D Fourier transformation. This process transforms the time domain signals into a frequency domain signals which can be processed by any image processing software.

Image files of 256x256 resolution have been produced for core samples flooded with both oil and  $D_2O$ . Each image file contains 256x256 pixels, where each pixel represents the area under the processed signal obtained by the NMR. The intensity of each pixel is in the range [0,255], where 0 represents the white gray-level, and 255 represent the black gray-level. A pixel can be represented as a volume element with dimensions  $\Delta X, \Delta Y, \Delta Z$  as shown in Figure 4.2.1. When the volume element is filled with fluid, the element is considered to be 100% saturated which corresponds to 255 pixel intensity. On the other hand, if the volume element is empty, the element is considered to be 0% saturated with any fluid. A zero saturation is correspondent to zero pixel intensity. Any other range of intensities between 0 and 255 can be represented by the amount of fluid contained in the volume element.

#### 4.2.5 Image Saturation

The experiment was set up so the oil phase is represented by the darker gray-level while the  $D_2O$  is represented by the lighter gray-level. When a cell has a gray-level of 255, a 100% oil saturation is encountered in that particular cell. The gray-level in a group of neighboring pixels must be averaged because a pixel does not represent a dimensional area. By grouping neighboring pixels together, an average saturation would have some meaning.

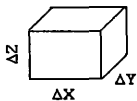


Figure 4.2.1a  
Volume Element Representing  
a Pixel.



Figure 4.2.1b  
Volume Element 100% Saturated  
A Pixel - 255 Intensity

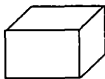


Figure 4.2.1c  
Volume Element 0 % Saturated  
A Pixel - 0 Intensity



Figure 4.2.1d  
Volume Element 50 % Saturated  
A Pixel - 152 Intensity

Figure 4.2.1  
Visualization of Pixel Intensity

The total sum of gray-level in a cell is the average volume of fluid in that cell. By summing up the volume of fluid in all the cells in the image, the average volume of fluid in the core can be obtained. Figure 4.2.2 shows an example of a 256x256 image where its pixels have been rearranged in a 3x3 cells.  $S$  represents the average saturation for the cell, while  $A$  is the area of that cell. For the arrangement shown in Figure 4.2.2, the integrated density of the image can be presented as:

$$\begin{aligned} \Psi = & A_1 S(x-1, y-1) + A_2 S(x-1, y) + A_3 S(x-1, y+1) \\ & + A_4 S(x, y-1) + A_5 S(x, y) + A_6 S(x, y+1) \\ & + A_7 S(x+1, y-1) + A_8 S(x+1, y) + A_9 S(x+1, y+1) \dots \dots (4.2.1) \end{aligned}$$

where  $\Psi$  is the integrated density, which is a function of both the area of the cell and the average intensity in that cell. Mathematically, the integrated density is the average intensity of pixels integrated over the area of the image.  $A$  is the area of the cell, and  $S$  is the average saturation of the cell. For a grid system composed of any number of cell, the total intensity equation can be modified as follows:

$$\Psi = \int_{y=0}^{y=j} \int_{x=0}^{x=i} A(x, y) S(x, y) \partial x \partial y \dots \dots \dots (4.2.2)$$

Saturation is the ratio of the calculated integrated density to the maximum integrated density. The maximum integrated density occurs when the density of the image is uniform and at maximum intensity. A 256 value is the maximum intensity in our case. The maximum integrated density can be represented as:



$A_1$ $S(x-1,y-1)$	$A_2$ $S(x-1,y)$	$A_3$ $S(x-1,y+1)$
$A_4$ $S(x,y-1)$	$A_5$ $S(x,y)$	$A_6$ $S(x,y+1)$
$A_7$ $S(x+1,y-1)$	$A_8$ $S(x+1,y)$	$A_9$ $S(x+1,y+1)$

Figure 4.2.2  
A 256x256 Image Averaged to a 3x3 Cell Image.

$$\Psi_m = \int_{y=0}^{y=j} \int_{x=0}^{x=i} 256 A_{(x,y)} \partial x \partial y \dots \dots \dots (4.2.3)$$

Where  $\Psi_m$  is the maximum integrated intensity. The ratio of equations 4.2.2 and 4.2.3 is a dimensionless number which is the saturation of fluid at the cross section where the image was taken.

$$S_o = \frac{\Psi}{\Psi_m} \dots \dots \dots (4.2.4)$$

Where  $S_o$  is the saturation of oil in the section.

#### 4.2.6 Example

This example is for an image taken from a longitudinal sectional area of a core. Figure 4.2.3 shows the image. The intensities shown in each cell of Figure 4.2.4 are averaged over an area of 20x15 pixels in the image of Figure 4.2.3.

An understanding of the numbers in Figure 4.2.4 is required before applying equation 4.2.4. In this study, the core was saturated with  $D_2O$ . Oil was injected in the core at constant rate from the right end of the core. The saturation is expected to be maximum at the right end, where the oil is injected at, and decreases towards the left direction as shown in Figure 4.2.3.

Oil saturation is represented by the numbers in Figure 4.2.4. The higher the saturation, the bigger the numbers that represent the average saturation in the cell. Figure 4.2.5 shows how the oil front moves. The

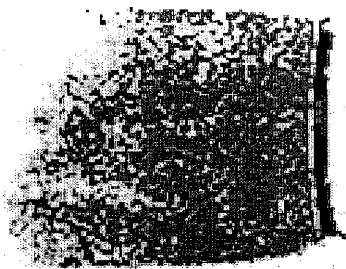


Figure 4.2.3  
NMR Image Used in Example.

3	3	9	75	119	124	117
3	3	65	97	134	142	148
3	13	122	136	162	165	158
3	12	130	138	159	169	159
3	44	122	124	165	173	168
3	40	119	141	165	165	152

Figure 4.2.4  
Average Intensities of Cells in Cross Sectional Area of a Core.  
Direction of Flow of Oil is from Right to Left.

3	3	9	75	119	124	117
3	3	65	97	134	142	148
3	13	122	136	162	165	158
3	12	130	138	159	169	159
3	44	122	124	165	173	168
3	40	119	141	165	165	152

Figure 4.2.5  
Saturation Front

saturation of oil in the center and bottom of the flow is higher than that at the top of the core. Sample preparation affects the behavior of fluid flow. Gravity, however, has an effect in the determination of the saturation distribution of oil.

The density plot of the longitudinal saturation averaged over the cross sectional area is shown in Figure 4.2.6a. The figure proves the maximum saturation is at the right end of the core and decreases to the left. The number of pixels as a function of gray-level is shown in Figure 4.2.6b. The figure shows that there are less pixels with low gray-level intensity. An estimate of the average saturation of oil in the given cross section can be found using the equations discussed above

$$\Psi = \int_{y=0}^{y=j} \int_{x=0}^{x=i} A_{(x,y)} S_{(x,y)} \partial x \partial y$$

$$= (20 \times 15) \times 117 + (20 \times 15) \times 124 + \dots + (20 \times 15) \times 3$$

$$= 1,246,500$$

$$\Psi_m = \int_{y=0}^{y=j} \int_{x=0}^{x=i} 256 A_{(x,y)} \partial x \partial y$$

$$= (20 \times 15) \times 255 + (20 \times 15) \times 255 + \dots + (20 \times 15) \times 255$$

$$= 3,213,000$$

$$S_o = \frac{\Psi}{\Psi_m} = 0.39$$

Figure 4.2.7 shows the saturation profile of the image in a 3D plot. As shown in the figure, the saturation of oil decreases from right to left.

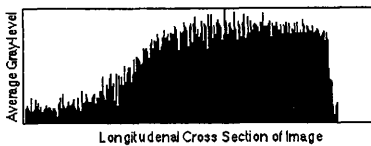


Figure 4.2.6a  
Density Plot of the Average Saturation

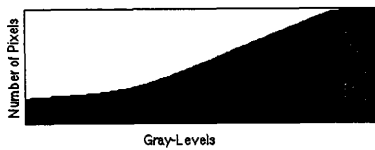


Figure 4.2.6b  
Histogram of the Saturation



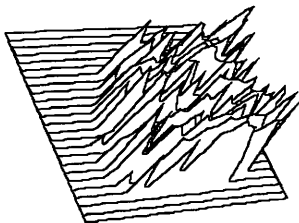


Figure 4.2.7  
Saturation Profile in a 3D Plot.

### **4.3 Relative Permeability**

This section presents the concept of relative permeability. The section begins with a review of the methods of measurements. The theory behind relative permeability is explained and an equation is then developed to relate the signal intensity from NMR images to the relative permeability in porous media.

#### **4.3.1 Multiphase Relative Permeability**

Multiphase relative permeabilities are extremely useful to calculating field performance for reservoirs being produced by both water and gas drives. Relative permeability data are needed for analyzing reservoirs which have partially lost their gas content and are being produced by water drive <sup>45</sup>.

Multiphase relative permeability measurements are rarely made with success. No reliable data are available in literature. Because of lack of data, it has not been possible to relate other rock properties to the relative permeabilities. It is necessary to measure experimentally relative permeability on the representative sample of the reservoir under considerations.

#### **4.3.2 Relative Permeability Measurements**

Methods available for relative permeability measurements can be grouped into two broad categories: One is capillary pressure methods, and the other is dynamic methods.

Hassler<sup>46</sup> developed a capillary pressure method in which capillary diaphragm assemblies were placed at each end of the core sample. These assemblies consisted of an outer ring diaphragm and a central disc diaphragm. Fluid flowed through the outer rings and

pressure drop was measured between central discs. Saturation was measured by collecting the displaced fluid.

This technique with a slightly modified form was used by Gares and Lietz, Fatt and Dykstra, and Corey et al to measure two and three phase relative permeabilities <sup>47</sup>. The technique is very complicated and therefore is not suitable for quick routine laboratory work. Each of these groups of researchers have published a theoretical models to calculate relative permeabilities from capillary pressure measurements and the calculated values fit their experimental data reasonably. Their models, however, are too simple to predict accurate quantitative permeabilities. A realistic model would involve parameters difficult to correlate.

The dynamic method, unlike capillary pressure method, does not use capillary diaphragm assemblies. All the fluid phases are allowed to flow simultaneously and pressure difference is measured away from the ends of the core sample to avoid influence of capillary forces at the ends. Flow rates are easy to measure, either by using constant displacement pumps, or by noting the rate of effluence of each phase at the downstream end.

Saturation value measurements are difficult in the dynamic method to measure. Various techniques have been used to measure saturation. These techniques are mentioned in section 4.2 of this Thesis and no need to repeat them here.

The electrical conductivity or resistivity method has been used for two-phase as well as three-phase relative permeability measurements by Leverett and Lewis. However, It has been shown that the resistivity of a rock partially saturated with a conducting fluid depends not only on its fluid saturation, but also on the spatial distribution of this fluid in the pore space. This influence is undesirable since fluid distribution is also a function of wettability of the rock.

Leverett and Lewis <sup>48</sup> have measured three-phase relative permeability, and their work is considered to be a classic. The electrical conductivity method was used for brine saturation determination and the Boyle's law method was used for gas saturation measurements. However, the method has certain disadvantages that can lead to inaccurate results.

A method using NMR imaging techniques of measuring two-phase relative permeability has been developed. The new method belongs to the dynamic method category where all the fluid phases are allowed to flow simultaneously.

#### **4.3.3. Advantages of NMR on Permeability Measurements**

The dynamic method of measuring relative permeability involves flowing different phases simultaneously. Many researchers have developed different procedures to measure the relative permeability of the flowing phases. All these procedures involve the same basic idea of flowing different phases simultaneously. The difference between these procedures is the way the fluid saturation is calculated.

The NMR technique of measuring relative permeability uses fluid saturation obtained from analyzing the NMR images. Relative permeabilities can be determined for any section in the core, allowing the study the variation of relative permeability to a fluid within the core sample.

The images produced from the NMR experiment can visually show the distribution of fluids in the cross section where the image was taken. This will help researchers to better understand the relationship between fluid distribution and relative permeability.

#### 4.3.4 Fluid Flow Theory

Darcy's law has been used to develop the flow equation. For a single phase, darcy's law states:

$$q = - \frac{kA}{\mu} \nabla P \quad \dots \dots \dots (4.3.1)$$

where  $q$  is the rate of flow,  $k$  is the absolute permeability of the porous rock,  $A$  is the cross sectional area of the flow,  $\mu$  is the viscosity of the flowing fluid, and  $\nabla P$  is the pressure gradient over the total length of flow. Pressure gradient for a horizontal system when ignoring the effects of gravity can be expressed as:

$$\nabla P = \frac{\partial P}{\partial x} \quad \dots \dots \dots (4.3.2)$$

In a two-phase fluid flow, two separate equation will be produced:

$$q_n = \frac{k_n A}{\mu_n} \nabla P_n \quad \dots \dots \dots (4.3.3a)$$

$$q_w = \frac{k_w A}{\mu_w} \nabla P_w \quad \dots \dots \dots (4.3.3b)$$

The subscripts  $w$ , and  $n$  stand for wetting phase ( $D_2O$ ), and non-wetting phase (oil).

The relative permeability to a fluid is defined as the ratio of effective permeability of the fluid to the specific permeability of the medium.

$$k_{rn} = \frac{k_n}{k} \quad \dots \dots \dots (4.3.4a)$$

$$k_{rw} = \frac{k_w}{k} \quad \dots \dots \dots (4.3.4b)$$

Where  $k_{rn}$  and  $k_{rw}$  are defined as the relative permeabilities to oil, and  $D_2O$  respectively. Substituting equations 4.3.4a and 4.3.4b into equations 4.3.3a and 4.3.3b we get:

$$q_n = \frac{k_{rn} k A}{\mu_n} \nabla P_n \quad \dots \dots \dots (4.3.5a)$$

$$q_w = \frac{k_{rw} k A}{\mu_w} \nabla P_w \quad \dots \dots \dots (4.3.5b)$$

By substituting equation 4.3.1 into equations 4.3.5a and 4.3.5b, we obtain:

$$k_{rn} = \frac{q_n \mu_n}{q \mu} \frac{\nabla P}{\nabla P_n} \quad \dots \dots \dots (4.3.6a)$$

$$k_{rw} = \frac{q_w \mu_w}{q \mu} \frac{\nabla P}{\nabla P_w} \quad \dots \dots \dots (4.3.6b)$$

Specific permeability is a rock property and is independent of the fluid flowing through the rock. Thus, viscosity and pressure gradient can be ignored in the equation 4.3.6a and 4.3.6b. The resulting relationship can be expressed as:

$$k_{rn} = \frac{q_n}{q} \quad \dots \dots \dots (4.3.7a)$$

$$k_{rw} = \frac{q_w}{q} \quad \dots \dots \dots (4.3.7b)$$

These two equations state that the relative permeability of a fluid is simply the ratio of the flow of that fluid when other fluids are present to the rate of fluid flow when only one fluid is present.

The flow rate of a fluid is a function of its saturation;  $q_o$  is a function of oil saturation. Thus, we conclude that the relative permeability of a fluid is a function of its saturation. Rate of fluid flow has been shown to have no effect on relative permeability as long as it does not create a saturation gradient. In the case of a water-wet rock, the relative permeability to oil is dependent on the oil saturation as well as the water saturation. The relative permeability to water, however, depends only on the water saturation.

#### 4.3.5 Measurements Procedure

Relative permeability can be measured for any cross sectional image in the core. The relative permeability obtained will be a function of the image saturation. In order to be able to determine the relative permeability-saturation relations, the following quantities need to be known:

- 1) Length of image where pressure was measured.
- 2) Cross sectional area of the core sample.
- 3) Viscosity of fluids.
- 4) flow rate of fluids flowing in the core sample.
- 5) Pressure across the image.
- 6) Saturation of the image.

When dealing with more than one image, five of the six mentioned variables are constant and depend on the rock and fluid physical properties. Image saturation, however, is changing from one image to the other. Thus, image saturation is the only factor that affects the change in relative permeability across the core.

#### 4.3.6 Permeability From Well Logging

Flow of oil and water in a water-wet porous medium can be expressed as <sup>49</sup>:

$$k_{rw} = \left( \frac{S_w - S_{wi}}{1 - S_{wi}} \right)^4 \dots \dots \dots (4.3.8)$$

$$k_m = \left( \frac{1 - S_w}{1 - S_{wi}} \right)^4 \dots \dots \dots (4.3.9)$$

When expressing the saturations in equation 4.3.8 and equation 4.3.9, the relative permeability for a cross sectional (2D) image can be written as:

$$k_{rw} = \left( \frac{1 - \frac{\int_{y=0}^{y=1} \int_{x=0}^{x=1} A_{(x,y)} S_{(x,y)} \partial x \partial y}{\int_{y=0}^{y=1} \int_{x=0}^{x=1} 256 A_{(x,y)} \partial x \partial y} - S_{wi}}{1 - S_{wi}} \right)^4 \dots \dots \dots (4.3.10)$$





**TABLE 4.3.1**  
**Relative Permeability as a Function of**  
**Gray-level ( $S_{wi} = 0.15$ )**

<b>Gray-level</b>	<b><math>K_{rw}</math></b>	<b><math>K_{ro}</math></b>
0	1.00	0.00
25	0.61	0.00
50	0.35	0.00
75	0.18	0.01
100	0.08	0.05
125	0.03	0.11
150	0.01	0.23
175	0.00	0.42
200	0.00	0.72
225	0.00	1.16
255	0.00	1.92

**TABLE 4.3.2**  
**Relative Permeability as a Function of**  
**Gray-level ( $S_{wi} = 0.20$ )**

<b>Gray-level</b>	<b><math>K_{rw}</math></b>	<b><math>K_{ro}</math></b>
0	1.00	0.00
25	0.59	0.00
50	0.32	0.00
75	0.16	0.02
100	0.07	0.06
125	0.02	0.14
150	0.00	0.29
175	0.00	0.54
200	0.00	0.92
225	0.00	1.48
255	0.00	2.44

**TABLE 4.3.3**  
**Relative Permeability as a Function of**  
**Gray-level ( $S_{wi} = 0.25$ )**

<b>Gray-level</b>	<b><math>K_{rw}</math></b>	<b><math>K_{ro}</math></b>
0	1.00	0.00
25	0.57	0.00
50	0.30	0.00
75	0.14	0.02
100	0.07	0.07
125	0.05	0.18
150	0.01	0.38
175	0.00	0.70
200	0.00	1.20
225	0.00	1.92
255	0.00	3.16

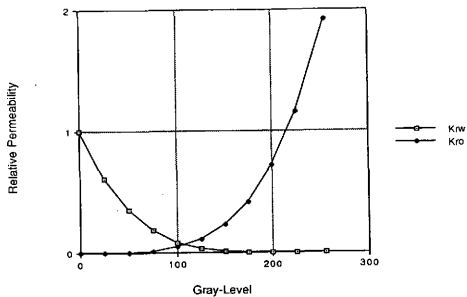


Figure 4.3.1  
Relative Permeability as a Function of  
Gray-level @ ( $S_{wi} = 0.15$ )

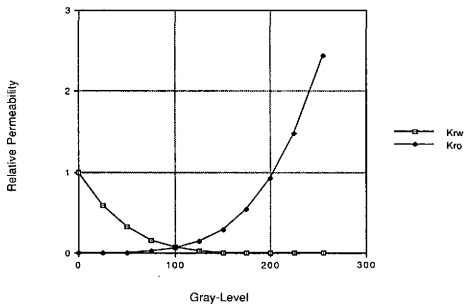


Figure 4.3.2  
Relative Permeability as a Function of  
Gray-level @ ( $S_{wi} = 0.20$ )

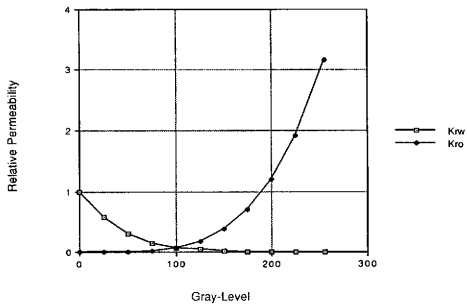


Figure 4.3.3  
Relative Permeability as a Function of  
Gray-level @ ( $S_{wi} = 0.25$ )

## 4.4 Imbibition Flooding

This section is a summary of imbibition flooding experiments that were performed using NMR techniques. The discussion also includes a summary of the experimental results.

### 4.4.1 Imbibition Using NMR Techniques

The NMR imaging technique is a multi-purpose investigative method that can be used to study the spatial distribution of changes in oil saturation. Different flood processes in cores can be easily studied using NMR imaging since this technique produces visual images of the saturation in the core. The NMR is not limited to one type of rock or one type of oil recovery process. It can be applied to a wide variety of rock types and enhanced oil recovery methods. Water imbibition is one of the oil recovery processes that is used in a fractured, low permeability reservoirs<sup>50</sup>.

### 4.4.2 Experimental Procedure

The water imbibition study was performed using a water-wet dolomite core. A 2 5/8" diameter and 5 7/8" long dolomite core with two lucite ends was wrapped with epoxy. The sample was placed in a core holder which has two inlet and one outlet openings as was shown in Figure 4.1.1. One of the inlet openings is for the non-wetting phase (oil) while the other is for the wetting phase (water). Since oil and water give ambiguous  $^1\text{H}$  NMR response,  $\text{D}_2\text{O}$  was used instead of water to obtain only  $^1\text{H}$  response for oil.

A fractured matrix face was simulated by indenting a 1/8" space into the lucite ends, creating an imbibition face. A  $\text{D}_2\text{O}$  flood was performed until maximum  $\text{D}_2\text{O}$  saturation was achieved. An oil flood



was performed to obtain maximum oil saturation. The mechanics of this process was shown in Figure 4.1.3.

Wetting phase ( $D_2O$  in this case ) will occupy the small pores and form a thin film over all of the rock surfaces in a water-wet rock initially at irreducible water saturation. Oil, the non-wetting phase, will occupy the centers of the large pores. This fluid distribution is shown in Figure 4.4.1. This distribution occurs because it is the most energetically favorable. Figure 4.4.2 is an image that shows the distribution of both oil and  $D_2O$  in the core.

Any oil placed in the small pores would be displaced into the center of the large pores by spontaneous water imbibition since the imbibition effect would lower the energy of the system. Figure 4.4.3 is an image of a core saturated with oil. The dark areas are the regions of maximum oil saturation. These regions are surrounded by a wetting phase (light color) which exist in the smaller pore spaces.

During the imbibition process several images were taken in three different sections: Cross sections, horizontal sections, and vertical section. These different image were taken to better visualize and understand the inside of the core sample and to be able to explain any unusual behavior of the flow pattern.

#### **4.4.3 Image Analysis**

Figure 4.4.4 through Figure 4.4.6 are the three types of images obtained from the NMR experiments. The horizontal image given in Figure 4.4.6 is further analyzed to understand the fluid distribution at that horizontal section. The average oil saturation of the image was calculated using the method discussed in section 4.2. The saturation was calculated to be 51%. Four saturation profiles across this image were plotted in Figure 4.4.7. The profiles show the decrease in average oil saturation towards the oil front.

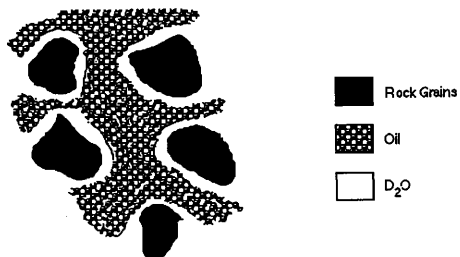


Figure 4.4.1  
Fluid Distribution in a Rock Sample

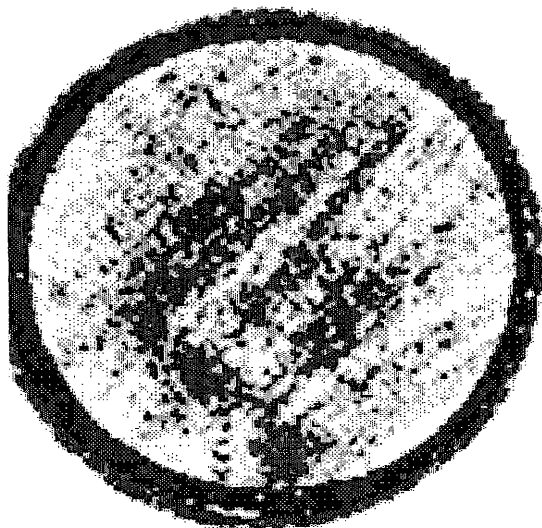


Figure 4.4.2  
NMR Image Showing the Distribution of Oil.

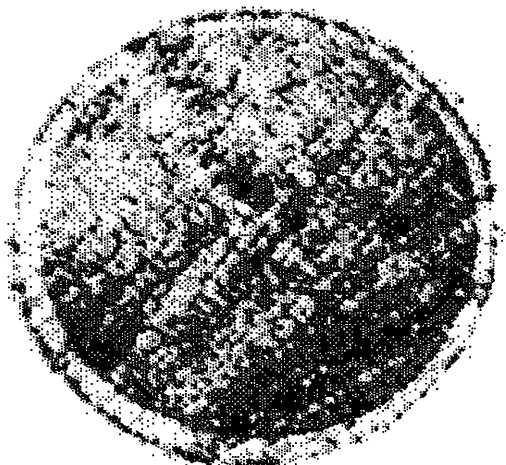


Figure 4.4.3  
NMR Image of Core Saturated with Oil.

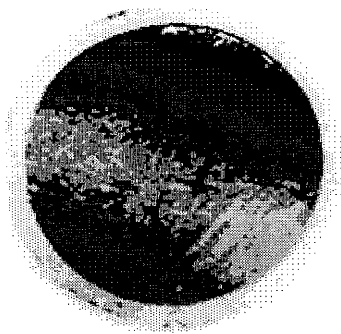


Figure 4.4.4  
Cross Sectional Image for a Core Flooded With Oil



Figure 4.4.5  
Image of a Vertical Section for a Core Flooded With Oil

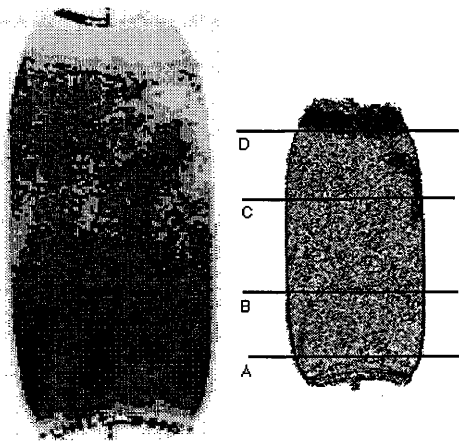


Figure 4.4.6  
Image of a Horizontal Section for a Core Flooded With Oil

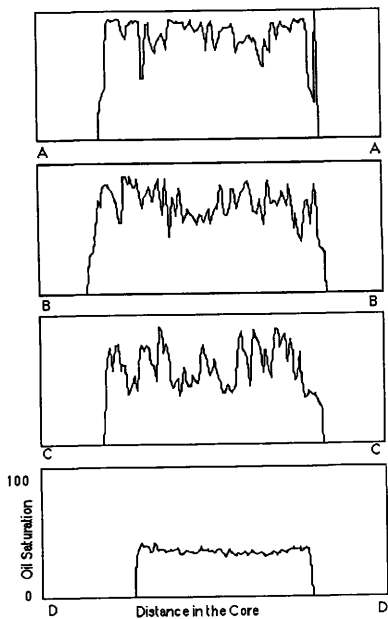


Figure 4.4.7  
Oil Saturation Profiles.



A longitudinal oil saturation profile also shows the decreasing oil saturation towards the oil front, Figure 4.4.8. A spike due to the small oil reservoir at the face of the core is also shown.

The region full of oil at the face of the core was used to scale oil saturation. Figure 4.4.9 shows an NMR signal taken across the length of the core. The area under the curve represents the volume of oil detected by the coil. The spike represents the oil maximum oil saturation in the oil reservoir at the face of the core.

Density variations across the core sample were calculated using the method discussed in section 4.2. Table 4.4.1 is a list of saturation changes as a function of distance inside the core sample. The saturations shown in the table were averaged over an area of 20x100 pixels. Saturation variations were plotted as a 3rd degree function of the distance inside the core. The third degree plot is shown in Figure 4.4.10 and it shows an average 2D change in oil saturation.

The distribution of oil in the core can easily be studied using both 3D plots of pixels intensity and contour maps of image density. Figure 4.4.11 is a 3D plot of the image saturation. The figure shows the changes of oil saturation across the core. Figure 4.4.12 is a contour map of the oil saturation in a resolution increment of 50 gray-levels. The contour map shows the regions of equal oil saturation in the image

#### **4.4.4 Imbibition Study**

The experiment started with a 100% saturated core sample. Oil in the indented space was displaced by  $D_2O$  at a rate of 0.2 ml/min. The pressure difference across the core sample is negligible, but the flow rate of  $D_2O$  remained constant throughout the experiment. Displaced oil was carried out of the core for measurement as shown in Figure 4.1.3.

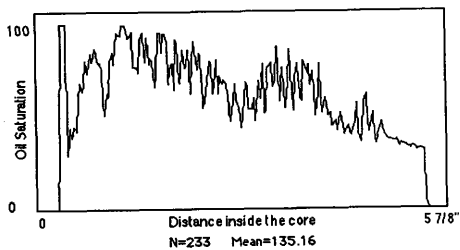


Figure 4.4.8  
Longitudinal Saturation Profile

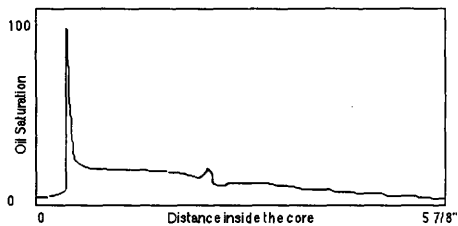


Figure 4.4.9  
NMR Signal Across the Length of the Core.

**TABLE 4.4.1**  
**Third Degree Saturation Function**

<b>Area</b>	<b>Mean</b>	<b>Position</b>
<b>pixel</b>	<b>intensity</b>	<b>pixels</b>
1940	130	10
2020	152	30
2080	158	50
2120	158	70
2060	145	90
2100	129	110
2060	142	130
1940	132	150
1840	104	170
1335	73	190

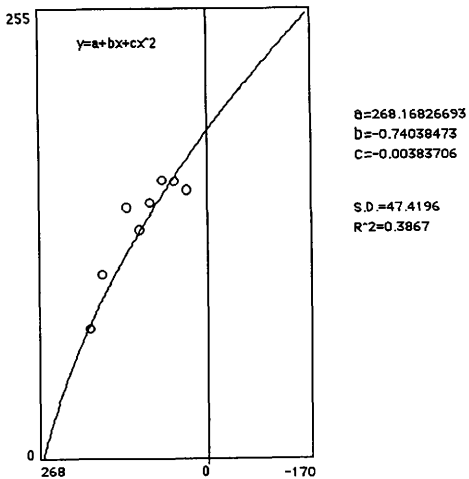


Figure 4.4.10  
Third Degree Function of Saturation Distribution.

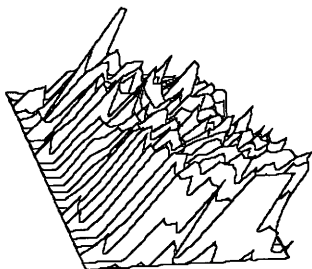


Figure 4.4.11  
3D Plot of Oil Saturation

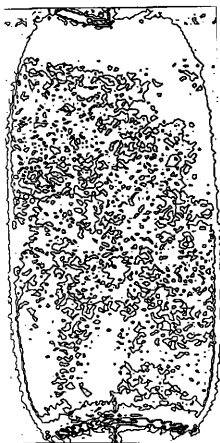


Figure 4.4.12  
Contour Map of the Horizontal Image.

NMR proton signals were taken at different times during the test. The decrease in oil saturation as  $D_2O$  was imbibed into the rock was calculated by subtracting NMR signal at the start of the experiment,  $t=0$ , from the signal at the time of interest. Residual oil saturation was calculated from the image taken when oil production by water imbibition was negligible.



## **CHAPTER V**

### **SUMMARY AND CONCLUSIONS**

This chapter summarizes the important points of this Thesis. Section 5.1 is a summary of the NMR imaging technique and its applications in fluid flow in porous material. A list of conclusions are presented in section 5.2. Section 5.3 end this Thesis with some recommendations.

#### **5.1 Summary**

High resolution NMR spectroscopy is a multi-purpose investigative technique that has been used in a variety of research. The NMR is based on detecting the proton of a molecule containing hydrogen. The signal obtained during the NMR experiment is proportional to the volume of hydrogen in the sample. The NMR techniques were used to detect the volume of oil contained in a porous media since crude oil contains Hydrogen.

The flow of fluid in a core can be visualized using the NMR techniques. The sample is concealed in a coil, and both of them were placed inside the magnet. An external magnetic field produced magnetization which was detected by the coil. The produced FID signal was then processed using Fourier transformation. The resulting data consisted of 256x256 matrices of even, positive integers. A program was developed to download and process the NMR raw data files. The program also reduces the noise level in the produced image. Public domain image processing programs were used to enhance the features of the NMR images. The public domain programs provided an easy and inexpensive means of enhancing the features of the image texture.

## 5.2 Conclusions

This NMR imaging research was conducted for three reasons: First, to better understand the NMR imaging technique. Second, to develop a new inexpensive method to download and process the NMR data. And finally, to apply the technique to fluid flow in porous material.

The following are some of the results of our research:

- 1) The NMR technique can be used to detect the amount of hydrogen in the sample. Since oil contains hydrogen, NMR can be used to study the saturation changes in core flooded with fluids.
- 2) NMR can nondestructively image a variety of chemical and physical properties of porous rocks and multiphase flow of fluid within their pores..
- 3) Flow performance and saturation can be determined microscopically. The thickness of the NMR image can be as small as 1 millimeter. A series of images in the core may be used to visualize the flow pattern.
- 4) NMR provides an easy way of imaging the interior of a rock saturated with fluids. Since the signals recorded are measures of the hydrocarbon exist in the rock, NMR can easily be used to determine the microscopic saturation of hydrocarbon in the rock.
- 5) NMR data files are usually processed using a Sun work-station which cost about \$100,000. The new technique enables us to use a Macintosh II system and public domain programs which reduce the cost by 5 fold.
- 6) A saturation equation was developed to calculate oil saturation in the image.
- 7) NMR techniques provide visual image of the fluid distribution in the rock.

### 5.3 Recommendations

When running the NMR experiment, the images must be taken under similar conditions in order to obtain a uniform signal level throughout the different images.

The signal obtained by the NMR coil ranges from 0 to 255. This signal needs to be scaled for oil saturation which normally ranges from 0 to 100%.

The program used to process the raw NMR data requires the user to input the noise level. When working with a multiple images, the noise level must be consistent to have a meaningful images.

A resolution of 256x256 was used when running the NMR experiment, However, a resolution of 512x512 could give better image features.

The signal obtained from the sample can be influenced by any change in the external magnetic field. The quality of the signal is influenced by the homogeneity of the magnetic field.

## NOMENCLATURE

$\epsilon$	Torque.
$h$	Plank's constant.
$\bar{H}$	Magnetic field
$H_0$	Magnetic field.
$l$	Spin quantum number.
$lh$	Angular momentum.
$T$	Temperature
$m$	Magnetic quantum number.
$\bar{M}_0$	Magnetization
$M_\Omega$	Decay of magnetization.
$M_z$	Magnetization recovered.
$\bar{\mu}$	Magnetic moment
$S_{wi}$	Initial water saturation
$S_{oi}$	Initial oil saturation.
$\gamma$	Gyromagnetic ratio.
$\omega_0$	Larmor velocity.
$\phi_0$	Larmor frequency.
$T_1$	Spin-lattice relaxation.
$T_2$	Spin-spin relaxation.
$T_2^*$	Decay rate constant in the rZ plane.
$(1/T_2')$	Mechanism which disperse magnetization in the Rz plane.
$\Delta\epsilon_m$	Torque produced by magnet.
$\Delta\epsilon_n$	Torque produced by nucleus.

## REFERENCES

- 1) Nuss, W.F., and Whiting, R.L.: "Techniques for Reproducing Rock Pore Spaces," *AAPG Bulletin* 4, Nov., 1947, 125-129.
- 2) Schaefer, W.: "Limestone Pore Space Study," a movie produced by the laboratories of Stanolind Oil and Gas Co., presented before Petroleum Division, AIME, Dallas, TX, October, 1948.
- 3) Calhoun, J.C., and Chatenever, A.: "Microscopic Behavior of Heterogeneous Fluids in Porous Media," a series of films presented before annual American Petroleum Institute Meetings in Chicago, Il., November, 1949; and Los Angeles, CA, November, 1950.
- 4) Williams, D.A.R.: *Nuclear Magnetic Resonance Spectroscopy, Analytical Chemistry by Open Learning*, London, John Wiley & Sons, Acol, 1987.
- 5) Vinegar, H.J.: "X-Ray CT and NMR Imaging of Rocks," *Journal of Petroleum Technology*, March 1986, 257-259.
- 6) Mansfield, P. and Morris, P.G.: *NMR Imaging in Biomedicine*, New York, Academic Press, Inc., 1982.
- 7) Fukushima, E. and Roeder, S.B.W.: *Experimental Pulse NMR*, New York, Addison-Wesley Publishing Company, 1981.
- 8) Wilson, M.A.: *NMR Techniques and Applications in Geochemistry and Soil Chemistry*, Institute of Energy and Earth Resources, Oxford, New York, Pergamon Press, 1987.
- 9) Ault, A. and Dudek, G.O.: *An Introduction to Proton Nuclear Magnetic Resonance Spectroscopy*, San Francisco, CA, Holden-Day, 1976.
- 10) Auther, H.: *NMR Spectroscopy: an Introduction*, Chichester, England, New York, Wiley, 1980.
- 11) Kemp, W.: *NMR in Chemistry*, London, Macmillan, 1986.
- 12) Fong, F.K.: *Theory of Molecular Relaxation*, New York, Wiley, 1975.

- 13) Muss, L.T., and Atkins, P.W.: *Electron Spin Relaxation in Liquids*, New York, Plenum Press, 1972.
- 14) Poole, C.P. and Farach, H.A.: *Relaxation in Magnetic Resonance*, New York, Academic Press, 1971.
- 15) Bracewell, R.N.: *The Fourier Transform and Its Applications*, New York, McGraw Hill, 1965.
- 16) General Electric: *CSI-II Operator's Manual*, New York, May 1986.
- 17) Shaw, D.: *Fourier Transform NMR Spectroscopy*, New York, Elsevier Science Publishing Company, 1984.
- 18) Smith, S.: *Magnetic Components: Design and Applications*, New York, Van Nostrand Reinhold, 1985.
- 19) Milgram D.L., and Rosenfeld A.: *Object Detection in Infrared Images*, New York, Digital Image Processing System, Springer-Verlag, 1982.
- 20) Muldner, T., and Steele, P.W.: *C as a Second Language For Speakers of Pascal*, Menlo Park, CA, Addison-Wesley Publishing Company, Inc., 1988.
- 21) Schildt, H.: *Advanced Turbo C*, programming series, second edition, New York, Borland Osborne/McGraw Hill, 1989.
- 22) Borenstein, P., and Mattson, J.: *Think C User's Manual*, Cupertino, CA, Symantec Corporation, 1989.
- 23) Serra, J.: *Image Analysis and Mathematical Morphology*, London; New York, Academic Press, 1982
- 24) Duff, M.J.B. and Fountain, T.J.: *Cellular Logic Image Processing*, New York, Academic Press, 1986.
- 25) Rasband, W.: *Image 1.13j User's Manual*, National Institute of Health, Research Service Branch, NIMH, New York, 1989.
- 26) Image Processing, Analysis, Measurement, and Quality: 13-15 Jan, 1988; Los Angeles, CA.: Part of SPSE's International Symposium and Exposition on Electronic Imaging Devices.
- 27) Kerzner, M.G.: *Image Processing in Well Log Analysis*, Boston, International Human Resources Development Corp., 1986.

- 28) Norris, C.L.: *Imagic*, the National Center for Supercomputing Applications at the University of Illinois at Urbana-Champaign 1989.
- 29) Montz, K., and Pinkerton, T.: *Enhance, the Professional's Tool*, New York, MicroFrontier, March 1990.
- 30) Rasband, W.: *Image1.13j*, National Institute of Health, Research Service Branch, NIMH, Chicago, IL, 1989.
- 31) Norman, M.L.: *Image Tool*, the National Center for Supercomputing Applications at the University of Illinois at Urbana-Champaign, 1988
- 32) Heintz, R.: *Layout*, the National Center for Supercomputing Applications at the University of Illinois at Urbana-Champaign, 1988
- 33) Krauskopf, T.: *DataScope*, the National Center for Supercomputing Applications at the University of Illinois at Urbana-Champaign, 1989.
- 34) NCSA: *NCSA Image*, the National Center for Supercomputing Applications at the University of Illinois at Urbana-Champaign, 1989.
- 35) Dake, L.P.: *Fundamentals of Reservoir Engineering*, New York, Elsevier Scientific Publishing Company, 1978.
- 36) Timmerman, E.H.: *Practical Reservoir Engineering*, Tulsa, Oklahoma, PennWell Publishing Company, 1975.
- 37) Richardson, J.G., Kerver, J.K., Hafford, J.A., and Osoba, J.S.: "Laboratory Determination of Relative Permeability," *Trans., AIME* **195**, 1952, 187-196.
- 38) Brownscombe, E.R. and Dyes, A.B.: "Water-Imbibition Displacement ... Can it Release Reluctant Spraberry Oil?," *Oil and Gas Journal*, Nov. 17, 1952, 264-265
- 39) Graham, J.W. and Richardson, J.G.: "Theory and Application of Imbibition Phenomena in Recovery of Oil," *Trans., AIME* **216**, 1959, 377-81.

- 40) Blair, P.M.: "Calculation of Oil Displacement by Countercurrent Water Imbibition," paper SPE 1475-G presented at the fourth Biannual Secondary Recovery Symposium of SPE in Wichita Falls, Texas, May 2-3, 1960.
- 41) Mattax, C.C. and Kyte, J.R.: "Imbibition Oil Recovery from Fractured, Water-Drive Reservoir," *JPT* (June 1962); *Petroleum Transactions*, AIME 225, 1962, 177-184.
- 42) Coomber, S.T., and Tiratsoo, E.N.: "The Applications of Radioactive Tracers Techniques to the Study of the Movement of Oil in Sands," *Jour. Inst. Pet.*, 36, 1950, 543.
- 43) Withjack, E.M.: "Computed Tomography for Rock-Property Determination and Fluid-Flow Visualization," paper SPE16951 presented at the 1987 SPE Annual Technical Conference and Exhibition held in Dallas. Sept. 27-30, 1987.
- 44) Asquith, G., and Gibson, C.: *Basic Well Log Analysis for Geologists*, the American Association of Petroleum Geology, New York, 1982.
- 45) Caudle, B.H., Slobod, R.L., and Brownscombe, E.R.: "Further Development in the Laboratory Determination of Relative Permeability," *Trans.*, AIME 192, 1951, 145.
- 46) Hassler, G.L.: "Methods and Apparatus for Permeability Measurement," *US Patent* no. 2, 345, 935, April 4, 1944.
- 47) Rapoport, L.A., and Leas, W.J.: "Relative Permeability to Liquid in Liquid-Gas Systems," *Petroleum Transactions*, AIME, 192, 1951, 83.
- 48) Fatt, I., and Dykstra, H.: "Relative Permeability Studies," *Petroleum Transactions*, AIME, 192, 1951, 249.
- 49) Timmerman, E.H.: *Practical Reservoir Engineering*, Tulsa, Oklahoma, PennWell Publishing Company, 1975.
- 50) Kleppe, J., and Morse, R.A.: "Oil Production from Fractured Reservoirs by Water Displacement," paper SPE 5084 presented at the SPE-AIME 49th Annual Fall Technical Conference and Exhibition, Houston, TX, Oct. 6-9, 1974.



## APPENDIX A

### ALGORITHM 1 Histogram Plot

```

Read the data file NAME
Open the data file NAME
Read Information INFO
Read BEGIN_ROW, END_ROW, BEGIN_COL, END_COL
SET  resx = END_COL - BEGIN_COL
      resy = END_ROW - BEGIN_ROW
Read an array of size resx by resy INTENSITY
Set DATA_MAX to maximum INTENSITY value
Perform a HISTOGRAM plot on the array INTENSITY
DO LOOP
    for ( INTENSITY=0; INTENSITY<DATA_MAX; increase by 1 )
        Set  HISTOGRAM_MAX to maximum number of
            pixels found in the HISTOGRAM plot
    END DO
END ALGORITHM

```

### ALGORITHM 2 Noise Detection

```

Set GRAY_LEVEL = 255
DO LOOP
    for ( i=BEGIN_ROW; i=END_ROW; increase by 1 )
        DO LOOP
            for ( j=BEGIN_COL; j=25; increase by 1 )
                Set NOISE_MAX = maximum value of INTENSITY
                Set NOISE = sum of pixels in NOISE_MAX area
            END DO
        END DO
    Set RESOLUTION = (resx*resy - NOISE)/GRAY-LEVEL
    Set AREA = 0
    Set COLOR = 0

```

END ALGORITHM

**ALGORITHM 3** Total Number of pixels

```

DO LOOP
  for (i=NOISE_MAX; i<DATA_MAX; increase by 1 )
    Set AREA = sum of pixels at each gray-level
    IF AREA is greater than or equal to RESOLUTION then
      {set AREA = 0}
      IF COLOR is less than 256 then
        {GRAY_LEVEL_ALLOWED (COLOR) = i}
        Set COLOR is equal to COLOR + 1
      END IF
    END IF
  END DO
END ALGORITHM

```

**ALGORITHM 4** Gray-level assignment

```

Set COLOR_MAX = COLOR
IF COLOR is greater than 256 then
  {COLOR = 255}
  Set GRAY_LEVEL_ALLOWED (COLOR) is equal to DATA_MAX
  Set COLOR = 255

DO LOOP
  for (i=BEGIN_ROW; i<=END_ROW; increase by 1)
  DO LOOP
    for (j=BEGIN_COL; j<=END_COL; increase j by 1)
    DO LOOP
      for (COLOR=0; COLOR<255; increase COLOR by 1)
      IF INTENSITY is less than GRAY_LEVEL_ALLOWED
        (COLOR) then
          {INTENSITY is equal to COLOR }
        END IF
      END LOOP
    END LOOP
  END LOOP

```

```
        END DO  
    END DO  
END DO  
END ALGORITHM
```

## APPENDIX B

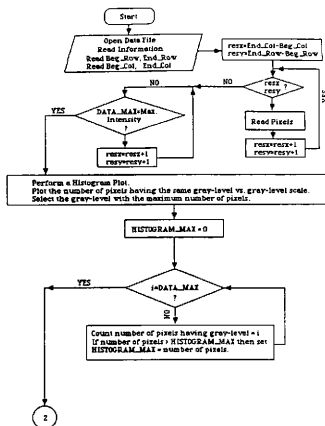


Figure B.1  
Flow Chart for Algorithm 1

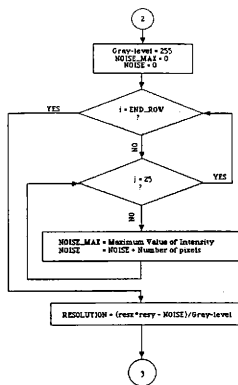


Figure B.2  
Flow Chart for Algorithm 2

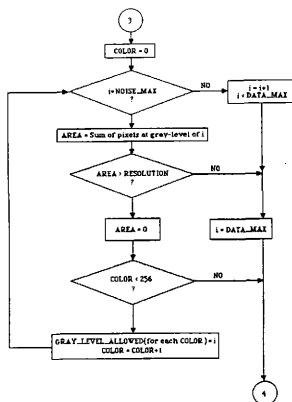


Figure B.3  
Flow Chart for Algorithm 3

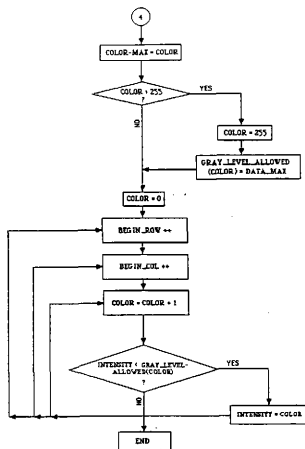


Figure B.4  
Flow Chart for Algorithm 4

**APPENDIX C**

This Appendix contains an algorithm of the function used to analyze the saturation front. The function traces the front of the oil or the region between the oil and water.

**Algorithm Fluid Front**

Read a 256x256 image

For each row DO

    Pickup the two pixels where the maximum intensity occurs.

    Set the intensity of the 256 pixels in the row to zero.

    set the intensity of the two pixels that were picked to 255.

CONTINUE{for the 256 rows}

END of Algorithm.



**VITA**

**Name:** Hassan I. Halimi

**Born:** July 21, 1966

**Parents:** Mr. and Mrs. Ibrahim Halimi

**Permanent Address:** 57/25 El-Sabra  
Gaza, Palestine

**Education:** Texas A&M University, College Station,  
TX. Bachelor of Science in Petroleum  
Engineering (August 1989).

Texas A&M University, College Station,  
TX. Master of Science in Petroleum  
Engineering (December 1990).